

AFRL-AFOSR-VA-TR-2023-0443

A White Matter Cable Theoretic Model of EEG Biorhythms

Pamela Douglas
UNIVERSITY OF CENTRAL FLORIDA
4000 CNTRL FLORIDA BLVD
ORLANDO, FL,
US

08/31/2023
Final Technical Report

DISTRIBUTION A: Distribution approved for public release.

Air Force Research Laboratory
Air Force Office of Scientific Research
Arlington, Virginia 22203
Air Force Materiel Command

REPORT DOCUMENTATION PAGE

PLEASE DO NOT RETURN YOUR FORM TO THE ABOVE ORGANIZATION.

1. REPORT DATE	2. REPORT TYPE	3. DATES COVERED	
20230831	Final	START DATE 20200315	END DATE 20230314

4. TITLE AND SUBTITLE
A White Matter Cable Theoretic Model of EEG Biorhythms

5a. CONTRACT NUMBER	5b. GRANT NUMBER	5c. PROGRAM ELEMENT NUMBER
	FA9550-20-1-0042	61102F
5d. PROJECT NUMBER	**5e. TASK NUMBER**	**5f. WORK UNIT NUMBER**

6. AUTHOR(S)
Pamela Douglas

7. PERFORMING ORGANIZATION NAME(S) AND ADDRESS(ES)
UNIVERSITY OF CENTRAL FLORIDA
4000 CNTRL FLORIDA BLVD
ORLANDO, FL
US

8. PERFORMING ORGANIZATION REPORT NUMBER

9. SPONSORING/MONITORING AGENCY NAME(S) AND ADDRESS(ES)	10. SPONSOR/MONITOR'S ACRONYM(S)	11. SPONSOR/MONITOR'S REPORT NUMBER(S)
Air Force Office of Scientific Research 875 N. Randolph St. Room 3112 Arlington, VA 22203	AFRL/AFOSR RTA2	AFRL-AFOSR-VA-TR-2023-0443

12. DISTRIBUTION/AVAILABILITY STATEMENT
A Distribution Unlimited: PB Public Release

13. SUPPLEMENTARY NOTES

14. ABSTRACT
EEG has provided unparalleled and non-invasive access to the temporal dynamics of the brain for nearly 100 years. EEG measures voltage fluctuations at the scalp that reflect the instantaneous superposition of electric dipoles in the brain. Localizing the neural generators of EEG is ill-posed mathematically because numerous combinations of (hidden) dipoles could lead to a particular (observed) scalp measurement. Solving this problem is crucial for treating seizure disorders, building neuroprosthetic devices, and laying the foundation for noninvasive brain computer interfaces (BCI). However, solutions to the EEG inverse problem classically restrict solutions to cortical gray matter in the brain. Our goal is to examine this long held fundament of EEG research by developing a novel computational model, and empirically testing this assumption by perturbing brain activity using a novel brain stimulation technique.

Here, we developed a novel cable computational model that includes axonal cross-talk, or ephaptic coupling. This model suggests that spikes traveling along white matter tracts may be more entrained or synchronized than previously thought, thus providing the opportunity to summate and contribute to scalp EEG recordings. Our empirical work supports this model prediction via rare depth recordings in white matter fibre tracts, and complementary brain stimulation evidence in humans. The preliminary analysis of these data is demonstrating very exciting results, confirming our model. With further empirical testing and model integration, this work will be poised to assess this long-held fundament of brain research, and move towards a functional and spectral density mapping of rhythms in the brain.

15. SUBJECT TERMS

16. SECURITY CLASSIFICATION OF:			17. LIMITATION OF ABSTRACT	18. NUMBER OF PAGES
a. REPORT	b. ABSTRACT	c. THIS PAGE		
U	U	U	UU	56

19a. NAME OF RESPONSIBLE PERSON	19b. PHONE NUMBER *(Include area code)*
HAL GREENWALD	703-588-8441

Standard Form 298 (Rev.5/2020)
Prescribed by ANSI Std. Z39.18

DISTRIBUTION A: Distribution approved for public release.

AFOSR, Dr. Hal. S. Greenwald

Abstract (publicly releasable)

EEG has provided unparalleled and non-invasive access to the temporal dynamics of the brain for nearly 100 years. EEG measures voltage fluctuations at the *scalp* that reflect the instantaneous superposition of electric dipoles in the brain. Localizing the neural generators of EEG is ill-posed mathematically because numerous combinations of (hidden) dipoles could lead to a particular (observed) scalp measurement. Solving this problem is crucial for treating seizure disorders, building neuroprosthetic devices, and laying the foundation for noninvasive brain-computer interfaces (BCI). However, solutions to the EEG inverse problem classically restrict solutions to cortical gray matter in the brain. Our goal is to examine this long held fundament of EEG research by developing a novel computational model, and empirically testing this assumption by perturbing brain activity using a novel brain stimulation technique.

Here, we developed a novel cable computational model that includes axonal cross-talk, or ephaptic coupling. This model suggests that spikes traveling along white matter tracts may be more entrained or *synchronized* than previously thought, thus providing the opportunity to summate and contribute to scalp EEG recordings. Our empirical work supports this model prediction via rare depth recordings in white matter fibre tracts, and complementary brain stimulation evidence in humans. The preliminary analysis of these data is demonstrating very exciting results, confirming our model. With further empirical testing and model integration, this work will be poised to assess this long-held fundament of brain research, and move towards a functional and *spectral* density mapping of rhythms in the brain.

DISTRIBUTION A: Distribution approved for public release.

TABLE OF CONTENTS

ACCOMPLISHMENTS SUMMARY 3

OBJECTIVE 1 6
Building a White Matter Cable Theoretic Model of EEG Biorhythms

OBJECTIVE 2 28
Empirically test theory in humans using transcranial ultrasound (TUS)

OBJECTIVE 3..... 40
Record Neural Activity *in vivo* in Rodent White Matter Tracts
(Originally Future Research)

DELIVERABLES / RESEARCH PRODUCTS 43
Journal Publications, Conference Papers, Conference Presentations

PARTICIPANTS & COLLABORATING ORGANIZATIONS 47

ACKNOWLEDGEMENTS 49

REFERENCES CITED 51

DISTRIBUTION A: Distribution approved for public release.

ACCOMPLISHMENTS

Summary
For the past century, EEG has provided unparalleled and non-invasive access to the temporal dynamics of the human brain. Throughout this time, EEG has been understood to measure current dipoles that arise from neocortical activity within superficial *gray matter* in the brain. The primary generators of EEG are thought to be post-synaptic potentials (ranging from 1-4 mV) traveling along large pyramidal cell dendrites in layer IV of the cortex. If true, then ~10^7 neurons in a spatially localized region (~6 cm^2) must fire quasi-synchronously to generate a signal of sufficient magnitude to be measured at the scalp. In contrast, action potentials (~100 mV) traveling along *white matter* tracts are orders of magnitude larger than dendritic inputs. However, they are traditionally assumed to be negligible contributors to EEG. This prevailing theory stems from the notion that action potentials are thought to be too asynchronous and fast to enable temporal summation, and thus will largely attenuate before reaching the scalp.

The purpose of this CCN award was to challenge this long-held assumption using a combination of computational modeling, and empirical data collected in human subjects. Our multimodal data collection included magnetic resonance imaging (MRI), EEG, and the use of a novel brain stimulation technique, transcranial ultrasound (TUS), capable of modulating neural activity in deep brain regions with elegant spatial precision and without altering neural activity in intervening brain regions.

Throughout this award, we acquired strong evidence in support of our theory that white matter signaling indeed contributes to EEG recordings. Our computational modeling results show that white matter topology can be used to predict the characteristic 1/f spectral signature observed in EEG. Our empirical data demonstrate that signaling along the large white matter corpus callosum tract either generates or is required for the generation of the prominent EEG alpha rhythm (8-12 Hz). This finding alone is poised to make a major impact in the field of neuroscience, because the alpha rhythm traditionally is thought to arise from occipital regions, and thalamo-cortical signaling. We extended this work to a rodent model, where we observed 1/f spectral densities, and synchronized spike volleys in electrophysiology recordings in white matter tracts, thus demonstrating the opportunity for white matter signaling to summate temporally and produce a signal with sufficient magnitude to be measured at the scalp.

Our research findings, described herein, are poised to make a major impact across the fields of Neuroscience, Psychology, and Medicine, and across both scientific research and clinical practice. Our results lay the foundation for novel EEG source localization solutions, which may be crucial for diseases such as epilepsy, and may lead to novel brain-computer interface (BCI) applications, and neural prosthetic devices. Integrating these findings may lead to a new way of conceptualizing neural coding and information processing in the brain, and thus development of novel Brain-Inspired AI algorithms.

DISTRIBUTION A: Distribution approved for public release.

The PI of this grant is incredibly thankful and honored for this support from the AFOSR, without which, this pioneering research would not have been possible. We were successful in completing all of the major objectives of the grant, and for each aim, we went beyond the proposed objectives, beginning work on future proposed studies, while developing new state-of-the-art engineering solutions to accomplish these goals. A summary of each objective and major accomplishments is provided below.

Objective 1: Building a White Matter Cable Theoretic Model of EEG Biorhythms
We proposed to develop a computational model of action potential spikes traveling along white matter fiber bundles in the brain using principles based on cable theory.

Results: We were successful in developing and testing our cable theoretic computational model of white matter signaling. Our model included contributions from both myelinated and unmyelinated neurons across a range of axonal calibers, reported in the literature. We then successfully derived morphological metrics from diffusion MRI (dMRI) images, using the large Human Connectome Project (HCP) data set. Using dMRI metrics as inputs, we used our white matter cable theoretic model in a *generative* capacity to predict 1/f spectral densities for each individual. Model predictions were then compared to empirical MEG data 1/f spectra for each HCP subject. For this objective, we proposed to explore the presence or lack thereof of axonal cross-talk in future work. Axonal cross-talk, or ephaptic coupling, between axons is surprisingly under studied. In tightly packed white matter, this cross-talk may explain how message passing in the brain is more synchronized than previously thought. We were successful at testing this future objective by embedding ephaptic coupling terms into our white matter cable theoretic model, and making 1/f predictions from dMRI geometric parameters (Figure 1a). Overall, this computational work demonstrates a tight relationship between white matter structure and functional 1/f biorhythms in the brain.

Objective 2: Empirically test our theory in humans using transcranial ultrasound (TUS)
Our objective was to establish proof of concept by collecting data in 20 human subjects including the following multimodal measurements: diffusion MRI, ASL, EEG, and TUS.

Results: We successfully collected 30 sessions of data in 24 subjects including baseline, during TUS, and after TUS while subjects performed behavioural tests specifically designed to determine whether (synchronized) white matter activity generates and maps to fundamental brain rhythms. To address the possibility that our data arose due to auditory evoked signals (confound), we developed novel solutions to implement a “sham” TUS condition to control for this potential confound. Our results show exciting evidence that suppressive TUS applied to the corpus callosum white matter tract induces alpha power desynchronization - consistent with our cable theoretic model (Figure 1b). Thus, the combined results from Objectives 1,2 demonstrate strong supporting evidence for our theory that white matter signaling contributes to EEG/MEG 1/f spectra. During this award, we developed new solutions to technical challenges that arose with our novel ultrasound brain stimulation technology. Ultimately, we required new equipment. The

DISTRIBUTION A: Distribution approved for public release.

PI of this grant is incredibly thankful to the Air Force for a DURIP award to purchase completely novel equipment to accelerate discovery of white matter -frequency mapping in humans.

Objective 3 (Originally Future Research) Recordings Neural Activity *in vivo* in Rodents
We proposed a future objective to take place after this award. This aim was to empirically measure white matter signaling *in vivo* with electrophysiology recordings in a rodent model.

Results: The PI of this grant (Dr. Douglas) partnered with a rodent electrophysiology lab (Dr. Andre Fenton, NYU), who provided in kind support for this project. We engineered new specialized electrodes to perform depth recordings in highly resistive *white matter* tracts - a novel approach. These rare recordings show exciting evidence - in support of our theory, specifically that coordinated spike volleys are evident white matter tracts in the rodent brain. Collectively, these results demonstrate that white matter signaling also displays a 1/f spectral signature, and importantly is more synchronized that previously thought, offering the potential for temporal summation and contribution to scalp EEG (Figure 1c).

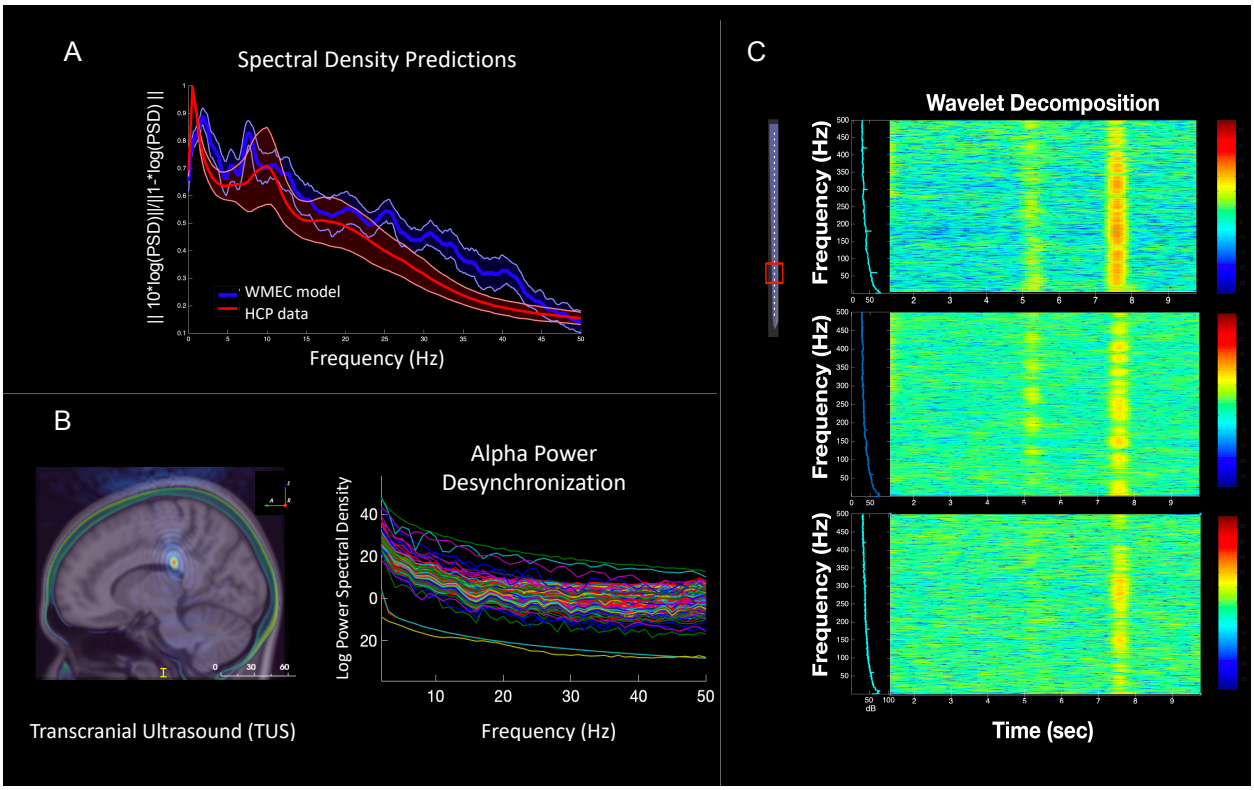


Figure 1: Summary of Major Accomplishments. A) Our white matter ephaptic coupling (WMEC) cable theory model was capable of predicting 1/f spectral densities observed in the Human Connectome Project (HCP) MEG empirical data. B) When transcranial ultrasound (TUS) is applied to corpus callosum (left), we observe a powerful desynchronization in EEG alpha power (right), consistent with our computational model. C) Wavelet decompositions derived from 3 spatially adjacent depth electrodes implanted in Long Evans rat white matter fiber tracts, superior to hippocampus. These recordings clearly show synchronized message passing, that is evident across both space and frequency.

DISTRIBUTION A: Distribution approved for public release.

OBJECTIVE 1: Building a White Matter Cable Theoretic Model of EEG Biorhythms

Abstract:

Since 1934, EEG has been thought to reflect synchronous neural activity from electrical sources close to the scalp. Within this classic view, inputs into apical dendrites in superficial gray matter represent the principal cortical generators of EEG or MEG observations. Here, we explore the possibility that neural signal transmission along (deeper) white matter fiber tracts may also contribute to EEG/MEG recordings. To do so, we develop a cable theory model of transmission along white matter fiber tracts that includes the presence of both myelinated and unmyelinated neurons in these fiber bundles. We then tested whether this model could generate 1/f spectral densities, widely observed in EEG/MEG data, within a recursive computation framework. We tested this model using diffusion MRI (dMRI) and MEG data derived from the Human Connectome Project (HCP) 1200 data set, both with and without the additional effects of ephaptic coupling. When applied in a generative capacity, our cable model with ephaptic coupling was capable of predicting realistic 1/f spectral signatures observed empirically in the HCP MEG data. We suggest spike volleys traveling along white matter tracts may additionally contribute to EEG/MEG observations, and that this line of inquiry may warrant further study.

I. Introduction

The existence of electrical phenomena in the brain was discovered more than a century ago when Richard Caton first observed visually evoked electrical currents in rabbits (Caton 1875). Over fifty years passed before the first demonstrations of human EEG by Berger, who described prominent “alpha waves” that were abolished with the eyes open (Berger 1929); (Stone and Hughes 2013). After additional research confirmed Berger’s observations (Adrian and Matthews 1934), EEG soon became a popular tool for studying the human brain in both health and disease, and numerous EEG signatures have since been mapped to cognitive and behavioral tasks e.g., (Lopes da Silva 2013).

Adrian & Mathews (1934) first suggested that EEG was caused by electrical sources close to the brain surface with a polarity oriented perpendicular to the scalp. However, the underlying neural mechanisms generating these electrical sources remained controversial for a period of time, partly due to the complexity of both the underlying neural dynamics and the attenuation and spread of signals as they propagate through the volume conductor (brain, cerebrospinal fluid, vasculature, skull, scalp) (Lopes da Silva, 2023). However, pyramidal neurons soon became widely accepted to be substantial generators of EEG or MEG signals (Lorente De Nó 1947), given their large size and their orthogonal arrangement with respect to the scalp.

Neuronal activity in brain causes time-varying transmembrane currents that can be measured in the extracellular medium. Although any type of transmembrane current (e.g., axonal) leads to deflections in both intracellular and extracellular field potentials, synaptic transmembrane currents have historically been considered to be the most prominent source of extracellular

DISTRIBUTION A: Distribution approved for public release.

current flow, electric dipoles, and EEG measurements (Buzsáki, Anastassiou et al. 2012). These postsynaptic potentials (PSPs) (either excitatory or inhibitory) evolve slowly due to their passive electronic conduction, and are created by transmembrane ionic currents that generate active sources-sink configurations in the extracellular medium (Lopes da Silva 2023) (see Figure 2).

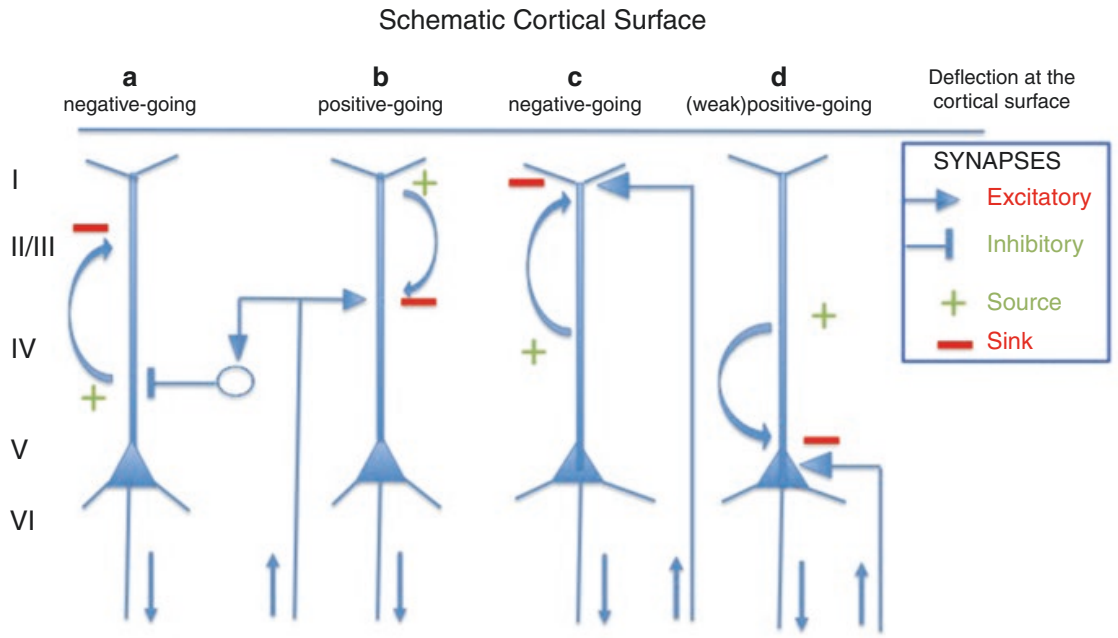


Figure 2: Schematic representation of the classic view of pyramidal cells being akin to "current dipoles" and the neocortical generators of local field potentials, reflected in EEG/MEG data. These dipoles can be generated by (a) inhibitory, or (b, c, d) excitatory post-synaptic potentials at different sites along the soma-dendritic memory of a pyramidal cell with the soma in laminar layer V of the cortex. The direction of extracellular currents is shown with curved arrows. The symbols representing excitatory and inhibitory synapses and electrical sources (+) and sinks (-) is indicated in the legend. Figure from Lopes da Silva (2023).

For decades, this "dipolar model" has remained the central theory for EEG generators, and has been widely cited and used to study both EEG and MEG (e.g., (Scherg 1990); (Nunez and Srinivasan 2006). It is worth noting that this long standing model implies a correspondence between EEG and extracellular currents reflected in local field potentials (LFPs). However, this relationship may be more complex. Reira et al. (2012) concurrently recorded EEG and LFPs in rat barrel cortex, and fount quadrupole and monopole current sources in addition to dipolar sources in cortical neurons (Riera, Ogawa et al. 2012). This work also showed that the extracellular potentials recorded did not sum to zero in the volume of a cortical column, as would be expected within the generally accepted model.

DISTRIBUTION A: Distribution approved for public release.

This classic view also requires that ~10^7 synapses be quasi-synchronously active in a spatially localized region to generate electric signals sufficient to propagate through the brain, dura, skull, and scalp and be measured by EEG (Cooper, Winter et al. 1965). In cortical gray matter, the strength and spatial extent of the current dipoles which must be quasi-synchronously active has been debated. In pioneering work, Cooper et al. 1965 concluded that a ~6 cm^2 area is required to produce observable EEG signals. More recently, studies using simultaneous MEG and subdural EEG recordings have suggested that ~ 4 cm^2 is sufficient to produce MEG signals e.g., (Oishi, Otsubo et al. 2002), though other studies have suggested that recruitment of even larger regions may be required (Ebersole 1997)**;**(Tao, Ray et al. 2005).

Although action potentials generate large voltage deflections, they have been considered negligible contributors to local field potentials and EEG. One of the primary reasons for this is that transduction along the axon is expected to be fast (~2 msec), and therefore unlikely to overlap sufficiently in time to produce signals of sufficient strength to be measured at the scalp (Andersen, Bliss et al. 1971). However, numerous non-synaptic processes including synchronous action potentials and spikes may also contribute to local field potentials and EEG (Buzsáki, Anastassiou et al. 2012). When spike after-hyperpolarizations are also considered, action potentials may also contribute to lower-frequency ranges as well (Einevoll, Pettersen et al. 2007).

Until recently, few empirical studies had noted the presence of unmyelinated neurons in human white matter using electron microscopy. This is partly because postmortem fixation can induce selective damage to unmyelinated neurons (Wang, Shultz et al. 2008). Newer fixation techniques have revealed that unmyelinated axons are present in significant quantities in white matter bundles in numerous species, even in long fiber crossings such as the corpus callosum (Caminiti, Carducci et al. 2013). Nearly 30% of callosal neurons were discovered to be unmyelinated in non-human primates (Liewald, Miller et al. 2014).

This new empirical observation has two important implications for computational modeling. First, the presence of unmyelinated neurons in white matter can greatly increase axonal packing density. At higher packing density, the external resistance is increased, thus altering signal transduction magnitude and velocity. Furthermore, higher packing density can create the opportunity for ephaptic coupling (Schmidt, Hahn et al. 2021).

Despite the long tenure of EEG use, there are surprisingly few studies that have examined the relationship between neuroanatomy and individual differences in EEG spectral properties. Nunez et al. (1978) noted an inverse relationship between head size and the spectral position of alpha peak (Nunez, Reid et al. 1978). However, Valdez-Hernandez et al. (2010) found no correlation between head size and the spectral position of alpha peak using EEG and MRI data. These authors did note a relationship between white matter architecture and peak alpha, suggesting that cortico-thalamocortical cycles might be modulating the alpha rhythm (Valdés-Hernández, Ojeda-González et al. 2010).

Recent studies from our group and others have investigated the relationship between white matter structure and EEG dynamics (Douglas and Douglas 2019); (Wolters, Anwander et al. 2006); (Güllmar, Haueisen et al. 2010). In the current work, we are interested in examining the

DISTRIBUTION A: Distribution approved for public release.

neuroanatomic determinants of EEG/MEG spectra through the lens of a white matter cable theory model.

This paper is organized as follows. First, we review the geometry of neuronal sources of electrical activity that are thought to subtend EEG measurement according to the classic description of open fields and pyramidal neurons in neocortical columns. We then review prior work and recent developments of generative models of EEG/MEG dynamics. Because fiber caliber and myelination play an important role in estimating the cable theoretic parameters and conduction velocities, we review neuroanatomic observations and more recent electron microscopy studies that informed the development of our white matter cable theory model. Lastly, we discuss the development of our white matter cable theoretic model, and the empirical data used for model evaluation.

Classic EEG Model: The Geometry of Measurement

The geometric consequences of the EEG measurement itself plays a key role in the putative generators of EEG signals. EEG measures instantaneous voltage differences at the scalp with respect to a reference or ground. Dipoles in large pyramidal neurons are thought to contribute most significantly to EEG measurements (Adrian and Yamagiwa 1935); (Eccles 1951), partly due to their arrangement within a critical column (Spruston 2008).

Electric dipoles arise when charges of opposite sign are separated by a distance. In the simple case of two opposite charges, ***q***, separated by distance, ***d***, measured from at distance of ***r,*** where the measurement distance is significantly larger than the charge separation (ie., r >> d), an approximation of the electric potential is given by:

$$V = \frac{kpcos\theta}{r^2} \tag{1}$$

Where the dipole moment p is,

$$\vec{p} = q\vec{d} \tag{2}$$

k is Coulomb's constant, and theta is the angle between **d** and **r** (Scherg 1990). Within this framework, radial dipoles, oriented approximately orthogonal to the scalp would contribute more significantly to the EEG measurement than tangential dipoles in sulcal regions (See Figure 3). Given the geometry of measurement, the classic generative model predicts that neural ensemble activity creates temporally overlapping currents leading to measurement of primarily the radial dipole fluctuations at the scalp.

DISTRIBUTION A: Distribution approved for public release.

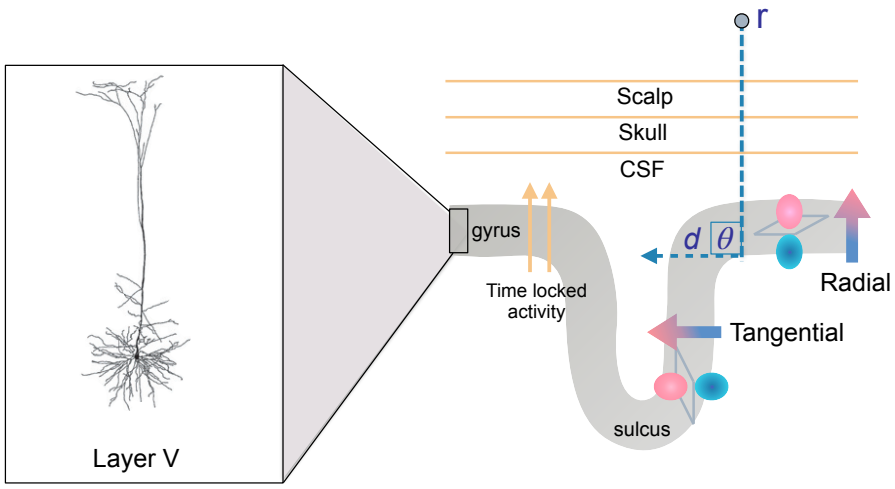


Figure 3: Geometry of measurement. Classic "dipolar model" view of EEG neuronal generators. Pyramidal cells (left) are principally localized to laminar layer V of the neocortex. Time locked activity from postsynaptic potentials produces dipole moments. Tangential dipoles, which are primarily in sulcal regions are not measured at the scalp due to the geometry of measurement. Radial dipoles in oriented orthogonal activity across numerous spatially extended neurons summates in gray matter, thus creating spatially extended radial and tangential dipole moments. Pyramidal neuron from Spruston (2008), dipole model inspired by Scherg (1990).

Generative Models of EEG

Numerous biophysically plausible models have been proposed for the generation of EEG signals (David and Friston 2003, Izhikevich and Edelman 2008) (Bastos, Usrey et al. 2012);(Moran, Pinotsis et al. 2013). These may be classified according to neuroanatomic scale and structure as: cortical, thalamic, or cortical-thalamic (Valdez-Hernandez et al. 2010). In this section, we focus on cortical models, as these have formed the basis for many inverse methods. We consider alternative approaches in subsequent sections.

The observation that archetypal neuronal circuits exist in repeated motifs throughout the brain (Creutzfeldt 1977), gave rise to a number of population density models that attempt to model dynamics within a representative cortical column. In this approach, populations of neurons are modeled as a single "cell" that represents ensemble activity from a specific class of neurons, sometimes referred to as the mean-field approximation (David and Friston 2003). Model structures (i.e., nodes and connectivity) are based on data ranging from neuronal morphology to stereotypic synaptic connections. Their dynamic interactions are typically formulated with coupled differential equations, and can be embedded observationally within a state-space model (e.g., DCM) (Moran, Pinotsis et al. 2013) or used for generative purposes (Roebroeck, Seth et al. 2011).

Initially, population density models had simple, deterministic architectures and utilized mean activation to approximate population dynamics as a point source (i.e., neural mass models (NMM)) (e.g., (Beurle 1956, Jansen and Rit 1995). Wilson and Cowan created a two

DISTRIBUTION A: Distribution approved for public release.

compartment model (Figure 4a), which was later expanded by Douglas and Martin (1991) to imbue cellular typologies with laminar specificity (Figure 4b)) (Wilson and Cowan 1972); (Douglas and Martin 1991). Even in these early models, the critical importance of tightly coupled excitation and inhibition was apparent. Ongoing experimental and theoretical work since have only further demonstrated that energy (ATP) consumption is lower (Sengupta and Stemmler 2014) and coding efficiency is higher in neural circuits with balanced excitation/inhibition (Denève and Machens 2016).

Neural field models (NFM), which have been developed in parallel with NMMs, explicitly incorporate a spatial dimension (Deco, Jirsa et al. 2008), by modeling how neuronal activity unfolds as continuous process along the cortical sheet (Pinotsis, Moran et al. 2012). Recent empirical evidence suggests that feedforward connections that link early areas to higher areas (e.g., LGN to V1), originate predominately in superficial layers and use relatively high frequencies compared to feedback connections (Bosman, Schoffelen et al. 2012). The canonical microcircuit (CMC) model, which has neural field properties, takes these laminar-specific spectral asymmetries into account (Bastos, Usrey et al. 2012) (Figure 4c-d)). Recently, the CMC model has been used as a measurement model within DCM to study excitation/inhibition imbalances during seizures (Cooray, Sengupta et al. 2015, Cooray, Sengupta et al. 2016). In the present work, we embed the CMC model within our cable model as a form of a delay within our recursive computing model, described below.

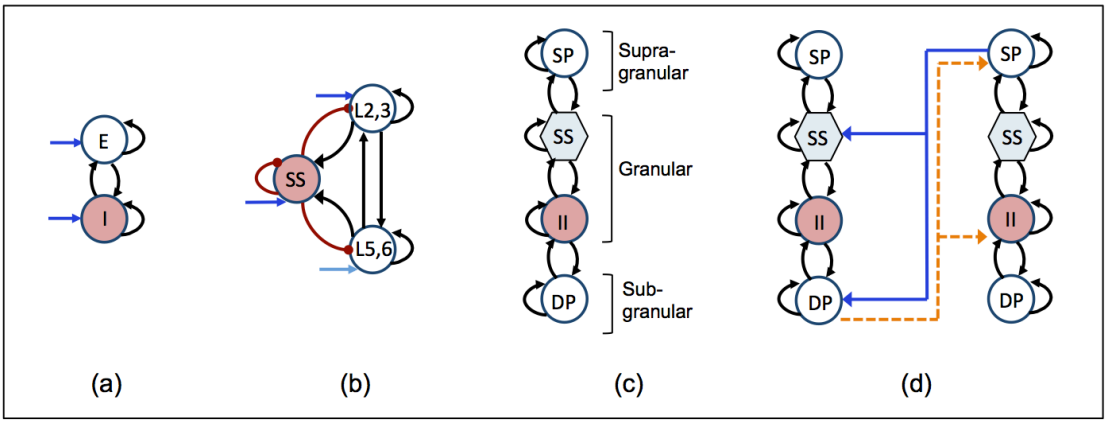


Figure 4: A) Wilson and Cowan (1972) modeled the proportion of excitatory (E) and inhibitory (I) cells firing per unit time via a sigmoidal subpopulation response function. Blue arrows indicate model inputs. B) The Douglas and Martin (1991) neural mass model comprises balanced excitation (black connections) and inhibition (red connections), adding laminar specificity for excitatory pyramidal cell populations in layers 2,3 (L2,3) and 5,6 (L5,6), and smooth inhibitory cells (SS). Feedforward connections from the thalamus target all populations with less emphasis on L5,6, (blue arrows). C) The canonical microcircuit model contains four neural populations: superficial pyramidal (SP), spiny stellate (SS), inhibitory interneurons (II), and deep pyramidal (DP) cells across different cortical layers. D) When the canonical microcircuit is connected into a network, feedforward connections (solid) originate from superficial layers, while feedback (dashed) connections emanate from deeper layers.

DISTRIBUTION A: Distribution approved for public release.

Fiber Calibre & Myelination

White matter connections are frequently categorized by length (Thatcher, Krause et al. 1986). Short distance (1-3mm) fibers are mostly thin and unmyelinated, connecting nearby cells within the *neuropil* of gray matter. Intermediate length fibers (10-30 mm) connect nearby cortical regions through a system of 'U' shaped fibers. The 'U' fiber system has an interesting geometry. The majority of the "U fibers" connect gyral regions, and the density of axonal fiber endings is significantly higher in gyral as opposed to sulcal regions. This geometry has led to debate over whether axonal 'pushing' or 'pulling' is responsible for inducing cortical folding during neurodevelopment in gyrencephalic brains e.g., (Nie, Guo et al. 2012). Long distance (30-170 mm) fascicles connect distant regions of the brain and are located deeper than, or below the 'U' fiber system. The relative abundance of these axon types is shown in Figure 4, and inspired by (Braitenberg 1978); (Braitenberg and Schuz 2002); (Wang, Shultz et al. 2008) (Figure 5).

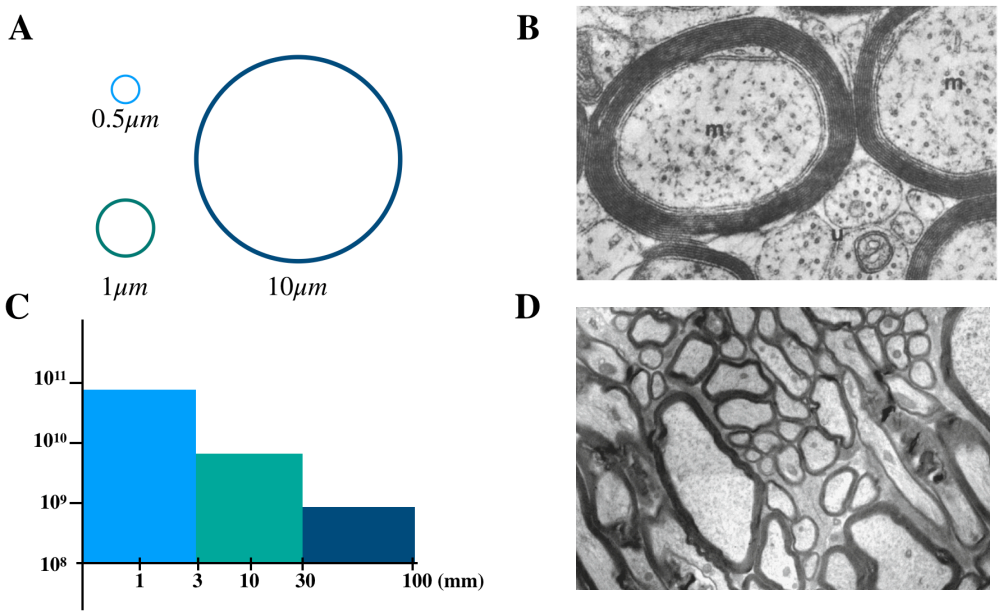


Figure 5: **A**) Typical diameters of unmyelinated (U), myelinated (M), and large myelinated (LM) neurons, inspired by (Wang et al. 2008). **B**) Stereotyped pattern of myelinated (m) and unmyelinated (u) axons in rabbit corpus callosum, electron micrograph from Waxman & Swadlow (1977) **C**) Relative abundance of axons according to length in brain, from Schuz & Braitenberg (2002). Note that under 1mm, neurons are typically unmyelinated, and have a faster conduction velocity than myelinated axons of this length Rushton (1951). **D**) In contrast to rabbit, electron micrographs from primate corpus callosum show a random arrangement across a range of diameters, from Liewald et al. (2014).

There is clearly a tight relationship between processing speed, axonal diameter, and myelination (e.g., (Waxman and Swadlow 1977). Therefore, it is surprising that relatively few studies have

DISTRIBUTION A: Distribution approved for public release.

quantified the density of fibers in fascicles, conduction delays, myelination, and axonal diameters in human. This is at least partly because the process of immersing a postmortem brain in fixative can induce tissue damage, particularly in unmyelinated neurons (Wang, Shultz et al. 2008). Nonetheless, a number of studies have demonstrated that unmyelinated axons appear to be present in significant quantities across a number of species, even in fascicles that connect distal regions of the brain (e.g., corpus callous) (Caminiti, Carducci et al. 2013). Nearly 30% of neurons in the corpus callosum were discovered to be unmyelinated in the primate brain (Liewald, Miller et al. 2014). Allometric scaling would predict the fraction of unmyelinated neurons to be slightly less in humans (Wang et al. 2008). However, a significant portion of unmyelinated neurons remains, and it is unclear what their purpose is if not to carry information. A histological example of this is shown in (Figure 5). It is also worth noting that unmyelinated axons are predicted to have *faster* transduction velocities, when the diameter is *smaller* than approximately 1μm (Figure 5). Therefore, it may be more efficient to use unmyelinated neurons for short distance communication (e.g., within the neuropil).

II. Methods

Our methods are organized as follows. First, we describe our computational modeling approach using principles from cable theory to model white matter signaling. We then describe data processing and statistical analysis of the Human Connectome Project data which was used for testing and evaluation of our computational model.

Cable Theoretic Model

Cable theory was initially developed for analyzing underwater telegraph transmission cables. In neuroscience, it was first applied to model the conduction of potentials in an axon (Hodgkin and Rushton 1946), and later gained popularity for modeling how passive electrotonic conduction spreads in a dendritic tree (Rall 2006). Prior to the 1980s, when applying nonlinear cable theory to axons, a common assumption was to assume that myelin was perfectly insulating (e.g., (McNeal 1976). In fact, one might question why biology did not make this so. However, neurons have nodes of Ranvier, or unmyelinated regions of the axon. When nodes of Ranvier are ignored, cable models typically provide an underestimate of the time constant, and an overestimate of the space constant (Basser 1993). Through the 1990s, “composite” cable models were developed conduction of action potentials, including nodes of Ranvier along the axon (e.g., Basser 1993).

In 2019, the PI of this award extended cable theory to model signal latency for single neurons in white matter fiber tracts (Douglas et al. 2019). Since this time, a number of studies have examined groups of action potentials, or spike volleys traveling along white matter (Sheheitli and Jirsa 2020); (Schmidt, Hahn et al. 2021). Cable theory has also been extended recently to model multi-physical properties of action potential propagation including electrical, mechanical, and magnetic field propagation in myelinated neurons with nodes (Wang, Wang et al. 2021).

Given that white matter microstructure is likely a heterogeneous fiber bundle, containing myelinated and unmyelinated neurons with varying axonal diameter, we would expect a diversity

DISTRIBUTION A: Distribution approved for public release.

of conduction delays. To calculate how potentials spread along white matter tracts, we build on work modeling conduction along "composite" cables, including the contribution of nodes of Ranvier in estimating propagation speeds. To do so, we first calculate space and time constants for each of the three axonal types. For myelinated axons of small and large type, we will use the formulation for a composite cable (Andrietti and Bernardini 1984). Within this formulation, the distribution of potential, *V(x,t)* may be calculated by the composite equation:

$$\frac{\partial^2 V}{\partial x^x} = (1-\chi)\left(\frac{\tau_m}{\lambda_m^2}\frac{\partial V}{\partial t} + \frac{V}{\lambda_m^2}\right) + \chi(x)\left(\frac{\tau_n}{\lambda_n^2}\frac{\partial V}{\partial t} + \frac{V}{\lambda_n^2} + \phi_{ion}(V,t)\right) \tag{3}$$

Where the first term represents the myelinated portion of the axon, and the second represents potential spread in nodal regions. The term χ selects the contribution of each term along the distance in space (x), and τ_m , τ_n and λ_m, λ_n are the time and space constants for myelinated and nodal regions, respectfully. To combine the effects of nodal and myelinated regions, we use the homogenized formulation from Basser et al. 1993 to calculate space and time constants as:

$$\lambda_c = \left(\left(1-\frac{\delta}{L}\right)\frac{1}{\lambda_m^2} + \left(\frac{\delta}{L}\right)\frac{1}{\lambda_n^2}\right)^{-1/2} \tag{4}$$

And

$$\tau_c = \lambda_c^2\left(\left(1-\frac{\delta}{L}\right)\frac{\tau_m}{\lambda_m^2} + \frac{\delta}{L}\frac{\tau_n}{\lambda_n^2}\right) \tag{5}$$

where λ_c is space constant for the composite cable in terms of λ_m and λ_n, the space constants, and τ_m and τ_n are the time constants for myelinated (m) and nodal regions (n), calculated classically from:

$$\tau_m = r_m c_m \tag{6}$$

$$\tau_n = r_n c_n \tag{7}$$

$$\lambda_m = \sqrt{\frac{r_m}{r_a + r_e}} \tag{8}$$

$$\lambda_n = \sqrt{\frac{r_n}{r_a + r_e}} \tag{9}$$

Here, r_m is the resistance of myelinated membrane (kΩ cm), r_n is the nodal resistance (kΩ cm), r_a is the resistance to axial current flow per unit length of membrane cylinder within the axoplasm (kΩ/cm). We use the nodal width, δ, of (~1x10^{-4} cm) from (Andrietti and Bernardini 1984). We used the length between nodes, L, observed in electron microscopy studies

DISTRIBUTION A: Distribution approved for public release.

(Arancibia-Caracamo 2017). We used the g-ratio relationship from (Hursh 1939), whereby inner axonal diameters are 70% of the ouster diameter in myelinated axons. A similar g-ratio observation was recently observed in mouse corpus callosum using scanning electron microscopy (Lee, Yaros et al. 2019). The membrane capacitance per unit length c_m in (μF/cm), can be calculated by:

$$c_m = \pi d C \tag{10}$$

Here, d is the axonal diameter, and C is the capacitance for a unit area of membrane, which is typically approximated as ~5 μF/cm^2 for nodal regions, 5x10^{-3} μF/cm^2 for myelinated regions (Tasaki and Freygang 1955). For unmyelinated neurons, we use the classic nonlinear cable equations for unmyelinated neurons. It is possible that the bundling of unmyelinated neurons within a fascicle containing myelinated neurons could create an insulating effect. For simplicity, we assume that this insulating effect is negligible. The time and space constants for small unmyelinated (u) axons can be calculated as:

$$\tau_u = r_u c_u \tag{11}$$

Table 1. Cable Model Parameters

Parameter	Value	Reference
Axon Diameter, **d**	Drawn from distributions for unmyelinated And myelinated neurons	Wang et al. (2008) Liewald et al. (2014)
Membrane Capacitance (**C_m**), Capacitance nodal regions (**C_n**)	5 μF/cm^2	Basser (1993)
Capacitance, myelinated regions (**C_y**)	5x10^{-3} μF/cm^2	Tasaki (1955)
Nodal Width δ	1x10^{-4} cm	Andrietti et al. (1984)
Length between Nodes,	1.5μm	Arancibia-Cárcamo et al. (2017)
Nodal Resistance area, **r_u**	0.02 kΩ cm^2	Schwartz et al. (1979)
Myelin Resistance area, **r_m**	100 kΩ cm^2	Schwartz et al. (1979)
Axoplasm resistivity, **r_a**	0.14 kΩ cm	Schwartz et al. (1979)
G-ratio, **g**	0.7	Hursh (1939)
Packing density ζ	0.8	Logothetis et al. (2007)

DISTRIBUTION A: Distribution approved for public release.

$$\lambda_u = \sqrt{\frac{r_u}{r_a + r_e}} \tag{12}$$

The resistance per unit area of an unmyelinated membrane, which is typically ~10^4 (Ω/cm^2), and R_a is the resistivity of the axoplasm ~140 Ω cm (Schwartz, Neumcke et al. 1979). An approximation to the spike propagation velocity can be calculated as (Jack, Noble et al. 1988):

$$\nu = 2\frac{\lambda}{\tau} \tag{13}$$

Table 1 provides a summary of parameters used in our cable model. A circuit diagram of our cable models for unmyelinated and myelinated neurons is shown in Figure 6 a,b. Axonal diameters were sampled from two empirical data distributions reported in the literature (see Figure 6 c,d).

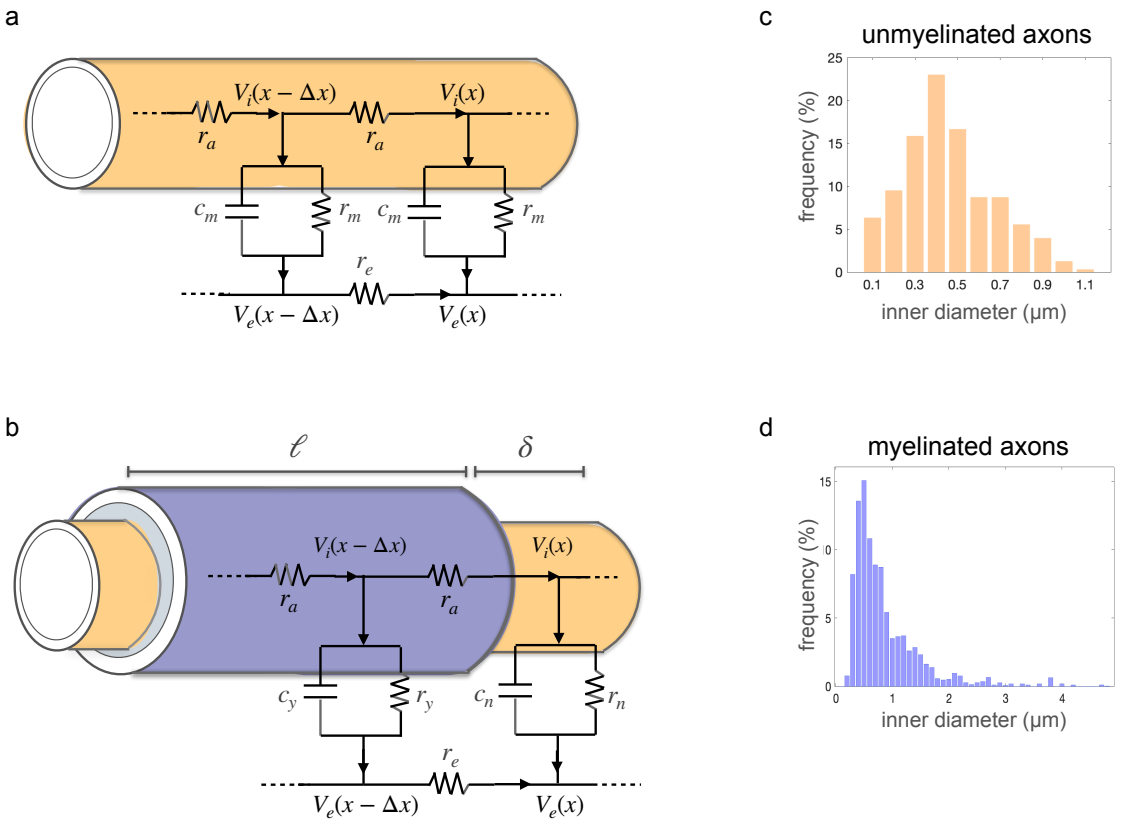


Figure 6: **A**) Circuit diagram representations for a section of an unmyelinated axon, where arrows indicate the direction of current; $\mathbf{r_a}$, $\mathbf{r_m}$, $\mathbf{r_e}$ are the axoplasm and membrane and extracellular resistance, $\mathbf{c_m}$ is membrane capacitance, and $\mathbf{V_i}(x)$ and $\mathbf{V_e}(x)$ are intracellular and extracellular voltage as **B)** Circuit model for composite cable shown for a portion of a myelinated axon, with nodal and myelinated resistance ($\mathbf{r_n}$,$\mathbf{r_y}$), and capacitance ($\mathbf{c_n}$,$\mathbf{c_y}$), respectively **C**) Axon diameter and frequency of observation reported in (Wang et al. 2008). **D**) Inner diameters for and frequency of observation from (Liewald et al. 2014). Diameters were sampled from these distributions for generative purposes.

DISTRIBUTION A: Distribution approved for public release.

Ephaptic Coupling (Axonal Cross-Talk)

Ephaptic coupling occurs when neurons interact with their neighbors, without forming synapses, by changing the electric potential of the extracellular medium. In cortex, extracellular resistivity is low (isotropic), and ephaptic coupling is typically treated as negligible. However, densely packed (anisotropic) white matter tracts have a higher resistivity (Logothetis, Kayser et al. 2007), particularly when the presence of unmyelinated neurons are taken into account with fiber packing density. Thus, it is possible that axon potentials traveling along parallel axons in white matter tracts may exert subtle effects on their neighbors (Schmidt, Hahn et al. 2021).

Seminal experiments in the 1940s (Katz and Schmitt 1940) (Arvanitaki 1942) demonstrated the phenomenon of ephaptic coupling *in vitro*. Signals traveling along *parallel axons* could interact with each other by changing the electric potential of the extracellular medium. Notably, it was observed that signals traveling along one axon could initiate axon potentials in passive neighboring neurons without forming synapses. However, these early experiments immersed neurons in highly resistive media such as paraffin, which is unlikely to represent the resistivity of biological axonal fibre bundles. In a subset of these experiments, the neurons were placed in moist air e.g. (Rosenblueth 1941). These experiments noted that axons in a bundle that began firing with an initial offset, would resynchronize, slowing down overall spike propagation velocities. More recent experiments have reproduced these results in intact brain slices, and found that signal re-entrainment occurs in white matter bundles, particularly at lower frequencies (< 8Hz) (Anastassiou, Perin et al. 2011). A number of computational models have shown action potential entrainment, through reseting small phase delays between parallel axons (Sheheitli and Jirsa 2020); (Anastassiou and Koch 2015). Ephaptic coupling has also been studied in the peripheral nervous system, where its effects are well documented both empirically and computationally (Schmidt and R. Knösche 2022).

In classic cable theory, the effects of extracellular voltage (V_e) are considered to have minimal effect on the membrane potential. In this classic cable theoretic case of zero ephaptic coupling, membrane potential is simply equal to the internal membrane potential, V_i, because $V_m=V_i - V_e$, and $V_e = 0$. When ephaptic coupling is considered, the external voltage fluctuations are no longer negligible.

Extracellular resistivity plays a critical role in the strength of ephaptic effects. Accurate measurements of resistivity, ρ, in either gray or white matter are technically challenging because they cannot be made with a single electrode (Logothetis, Kayser et al. 2007). Experiments using the 4-point method have generally confirmed that (isotropic) gray matter has a relatively low resistivity, and therefore minimal ephaptic effects. However, white matter is anisotropic. In this sense, the geometry of the resistivity is important. In the axial dimension (or direction of fibers), the resistivity in white matter is very low. Conversely, the transverse resistivity is extremely high. The extracellular electric potential V_e, represents the cumulative superposition of all neighboring cellular processes taking place. We therefore used the "test neuron" approach proposed by Goldwyn & Rinzel (2016) to examine our model predictions whilst varying the

DISTRIBUTION A: Distribution approved for public release.

strength of ephaptic coupling. This test neuron approach in turn, yields an additional term for space and time constants:

$$\kappa = N \frac{r_e}{r_a} \tag{11}$$

Where *N* is the number of neurons in the population (Goldwyn and Rinzel 2016). . We used the relationship from (Sheheitli and Jirsa 2020), to compute external resistance:

$$R = \frac{r_a}{r_e} = \frac{1}{\rho} \frac{A_e}{A_a} \tag{12}$$

Here A_e and A_a are the cross-sectional areas of extracellular space and axonal space, and $\boldsymbol{\rho}$ is the ratio of extracellular to intracellular resistivity. This ratio is generally thought to range from 1-4 (Sheheitli and Jirsa 2020). The coupling parameter can therefore be expressed in terms of the packing density, $\boldsymbol{\zeta}$, and the resistivity ratio:

$$\kappa = \rho \frac{\zeta}{1 - \zeta} \tag{13}$$

Our goal was to use our model in a generative capacity to make spectral decompositions while varying the effects of ephaptic coupling.

Human Connectome Project (HCP) Data

The Human Connectome Project (HCP) has made a high-quality multimodal brain imaging database publicly available (Human Connectome Project, 2017). This large database (~40 Tb) provided the opportunity to test our cable theoretic computational model and the ability to make structure-function predictions. Testing the cable model required geometric parameters derived from white matter (model inputs), and functional measurements of brain activity to compute spectral densities (model outputs). Therefore, we used diffusion MRI data (dMRI) as our model inputs to make predictions, and used magnetoencephalography (MEG) data to evaluate our model predictions. A subset of 95 subjects from the HCP1200 release met our inclusion criteria having data available in both modalities.

Diffusion MRI Data

Multi-shell dMRI data from 95 subjects in the HCP 1200 data set were included in our analysis. Multi-shell images were acquired on a Siemens Skyra scanner over three b-values (1000, 2000, 3000 s/mm^2) with an isotropic voxels size of 1.25 mm (Sotiropoulos, Moeller et al. 2013). We used the HCP pre-processed data (Glasser, Sotiropoulos et al. 2013), where diffusion imaging distortion corrections, and images were aligned to MNI152 space.

We used DSI Studio to perform tractography analysis on these data to extract topological metrics. Geometric and shape metrics were derived for all white matter tracts in the JHU White Matter Atlas for each of the included HCP subjects. Derived measures that were used in our analysis included: number of tracts, mean path length (mm), curl, diameter, volume, and total surface area. A multi-shell diffusion scheme was used, and the b-values were 1000 ,2000 and

DISTRIBUTION A: Distribution approved for public release.

2995 s/mm^2. The number of diffusion sampling directions were 90, 90, and 90, respectively. The in-plane resolution was 1.25 mm. The slice thickness was 1.25 mm. The diffusion tensor was calculated.

Magnetoencephalography (MEG) Data

We analyzed resting state MEG (R-MEG) recordings using FieldTrip, a Matlab toolbox, in combination with additional analysis functions, referred to as the "megaconnectome" pipeline, designed specifically for the HCP data set. Our cable theoretic model then was leveraged in a generative capacity - to predict spectral densities, and compared these to the HCP *resting state* MEG data. Thus, the model inputs were structural and geometric properties of white matter, and the model predictions were compared with functional MEG 1/f spectral densities.

Spike Volleys and Frequency Estimates

Our goal was to make whole-brain spectral density predictions using our white matter cable model. To do so, we used our spike velocity estimates generated by our cable model along with fiber lengths derived from the HCP data set to estimate the time required to travel in a single direction for all white matter tracts. This was computed for all axonal diameters sampled from myelinated and unmyelinated distributions. Arrival times at the terminal end served as inputs into the CMC model, which effectively served as a delay function before another spike then traveled in the reverse direction along each tract. Thus an estimate for frequency can be calculated as the inverse of the time required to make a complete cycle, or traversing the length of a given fascicle once in each direction.

We simulated MEG spectra using a 1000Hz sampling rate for 5 seconds across all fiber tracts. For each tract, we assumed that the number of axons, N, was proportional to the tract volume. We used the relationship reported by (Braitenberg and Schuz 2002) to estimate the total volume of short association U-fiber tracts as 90% of the total volume across all other tracts. We used our model first to generate time series data, and then calculated power spectral densities across the superposition of all time series data.

III. Results:

After extracting shape parameters from the dMRI data within the HCP data set, we first sought to examine whether any of the structural and geometric parameters of the dMRI data, showed 1/f characteristics. We found no evidence for a log-linear relationship between geometric parameters such as mean tract length, and tract volume (Figure 7). The relationship between fiber length and volume appears to be complex and nonlinear. Supplemental Table 1 provides the mean and standard deviation of tract lengths and volumes derived from the HCP dMRI data.

DISTRIBUTION A: Distribution approved for public release.

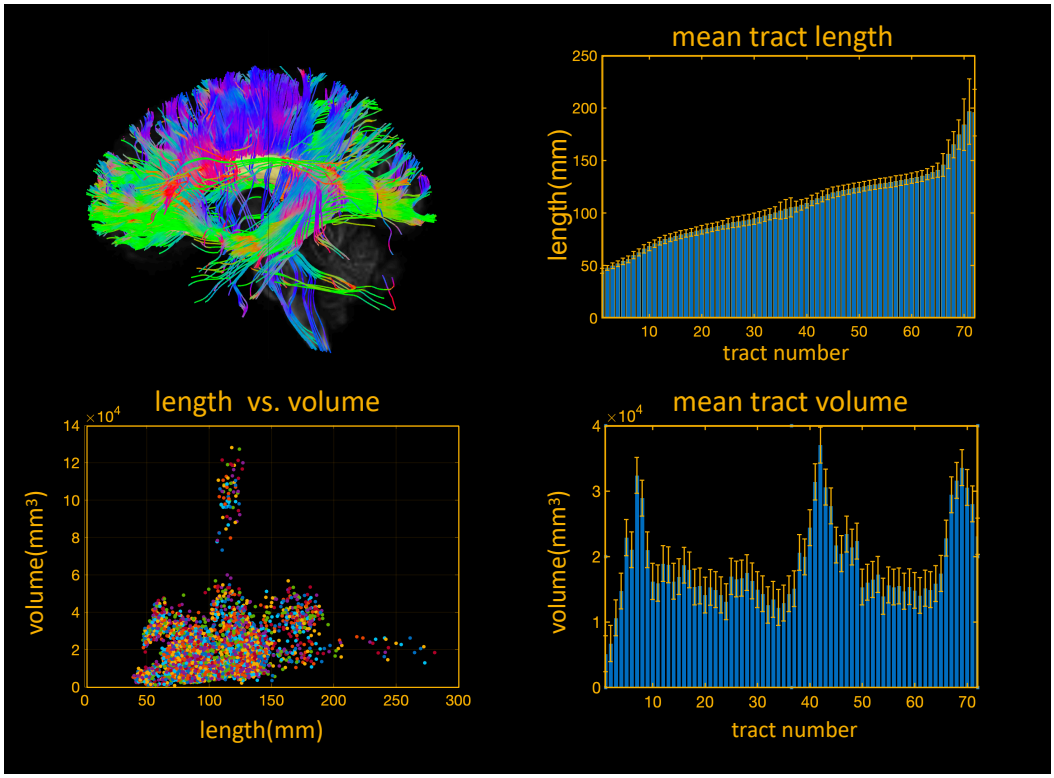


Figure 7: Geometric parameters derived from HCP dMRI data. (Top left) Representative dMRI image, sagittal view. (Top Right) Mean tract length (mm) with standard deviations shown, sorted according to length, and the corresponding volumes (mm^3) for those tracts (Lower Right). (Lower Left) Relationship between length and volume appears complex and non-linear.

Select estimates of the space and time constants and velocity estimates for selected axonal diameters in our cable model are shown in Table 3, for certain axon inner diameter ranges in the case where ephaptic effects have been considered negligible. Figure 8 shows the corresponding latency estimates for unmyelinated, myelinated, and large myelinated axons in the corpus callosum. These latency estimates correspond to the spike propagation travel time required for a signal at one end of the white matter tract to reach the synaptic terminal on the other hemisphere, traveling in a directional sense (Figure 8, top right).

Table 3: Selected Cable Model Estimates

	Diameter (μm)	**τ (msec)**	**λ (cm)**	**ν (m/sec)**
Unmyelinated	0.5	0.1	0.00084	0.27
Myelinated	1	0.192	0.0537	5.58
Large Myelinated	10	0.192	0.170	17.6

DISTRIBUTION A: Distribution approved for public release.

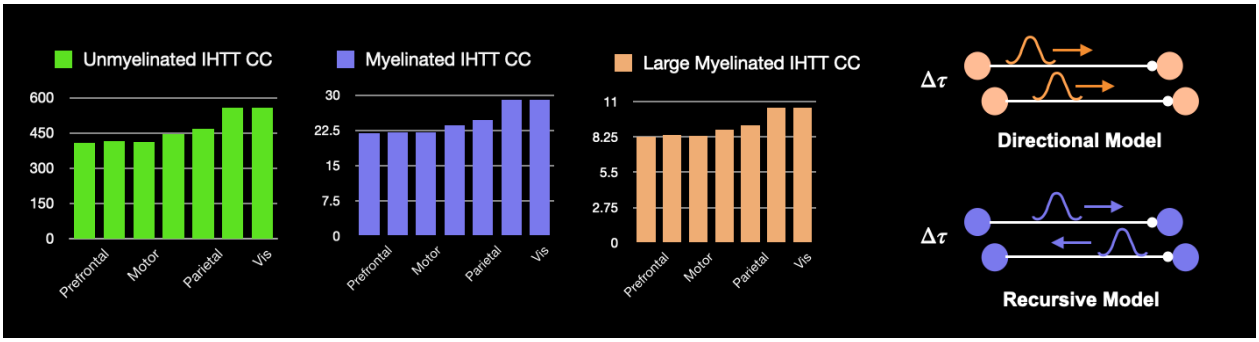


Figure 8:. (Left) Latency estimates for spike propagation in corpus callosum for unmyelinated, myelinated, and large myelinated fibers. These estimates represent the time for a spike to travel from its origin at one end of the tract to its synaptic terminal. (Right) Recursive computation is widely observed in the brain. Our spectral estimates were generated by estimated the the total time to travel in one direction, and then return after a delay modeled by the classic canonical microcircuit model.

To explore how the effects of ephaptic coupling would alter spike propagation velocity, and therefore latencies, in unmyelinated and myelinated neurons, we varied the parameter, ρ, in our model. Figure 9 shows that spike propagation velocities increase with axonal inner diameter for both myelinated and unmyelinated neurons, as expected. As the resistivity ratio, ρ, increases our white matter ephaptic coupling (WTEC) model generates reduced spike propagation velocities, which has also been noted in recent computational studies of ephaptic coupling (e.g., Schmidt et al. 2021). This velocity attenuation appears to be nonlinear in both myelinated and unmyelinated neurons. Increasing ρ also reduced the space constant for both unmyelinated and myelinated neurons across a range of inner axonal diameters drawn from empirical distributions (Figure 9, lower panel).

The distance that signals travel down neurons is expected to fall off inversely with respect to the space constant. Increasing ρ, and correspondingly the strength ephaptic coupling, we observe that the membrane potential distribution along the axon decays more rapidly (Figure 10). When ρ and packing density are very small, the coupling term, κ, approaches zero. In computational experiments of ephaptic coupling in the medial superior olive (MSO), plausible values for the ephaptic coupling parameter were estimate to reach as high as 15 (Goldwyn and Rinzel 2016). To explore how the strength of ephaptic coupling alters spectral densities produced by our model, we generated spectral densities across a range of κ values. Figure 11 shows the group average MEG spectral density derived from all subjects in the HCP data set, along with spectral density estimates generated by our model (blue).

DISTRIBUTION A: Distribution approved for public release.

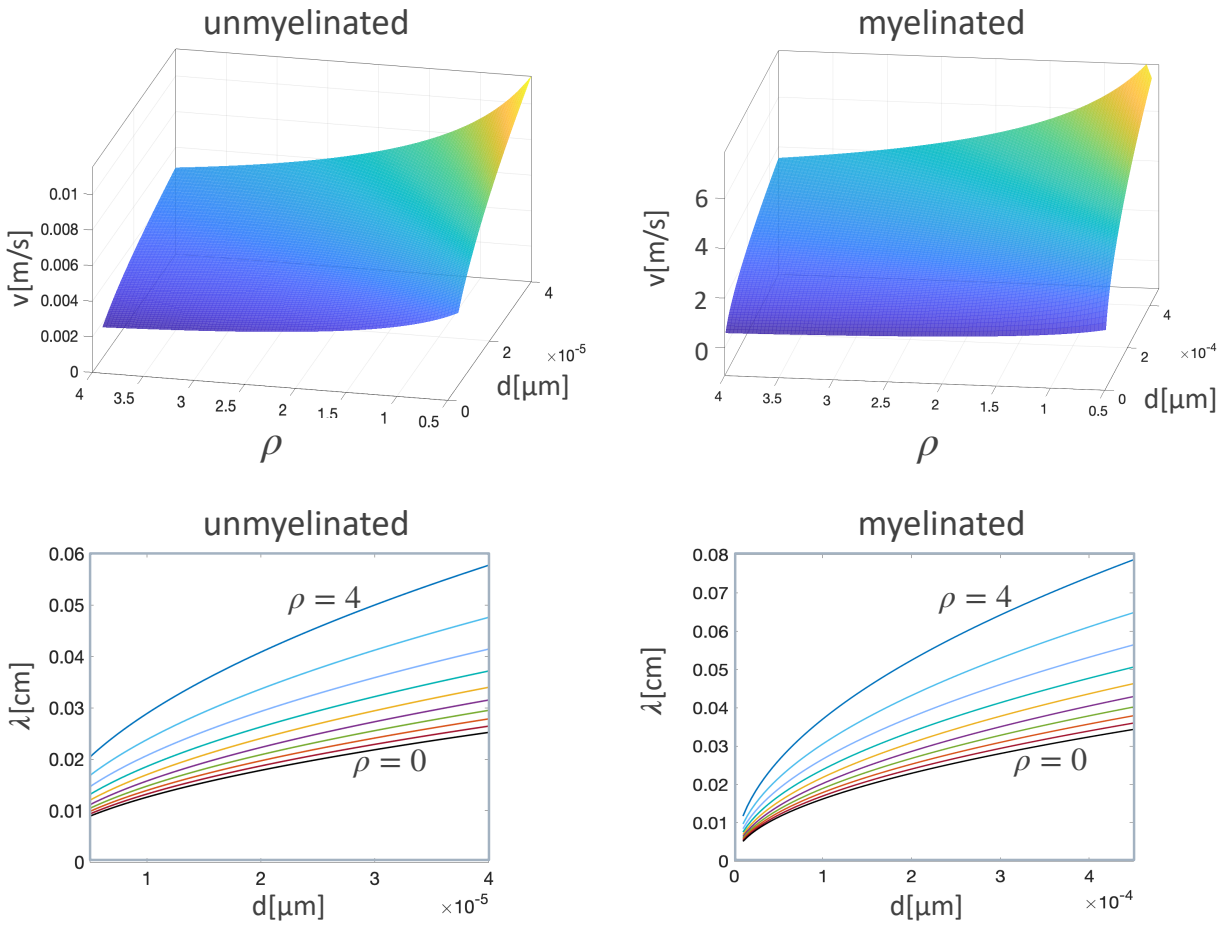


Figure 9: (Top) Spike propagation velocity estimates across varying inner axonal diameters, d, and while varying the ρ parameter, which modulates the strength of the ephaptic coupling parameter for unmyelinated (top left) and myelinated axons (top right). (Lower) The effects of varying the ρ parameter on the space constant λ across inner axonal diameters for unmyelinated (lower left) and myelinated neurons (lower right).

To examine the goodness of fit of the model predictions, we examined the cross-correlation between the empirical MEG data and model predictions. The model with zero ephaptic coupling effects had the lowest cross-correlation score. In the absence of ephaptic coupling, the higher frequencies dominated the spectra, and did not resemble a log-linear 1/f signature characteristic of EEG/MEG signals. As the ephaptic strength was increased to10, we begin to observe a log-linear relationship between power and frequency, yet without a distinct alpha peak in the expected range of 8-12 Hz. Increasing the ephaptic strength to 12.5, produced an alpha peak in the expected frequency range. At ephaptic coupling strength as high as 15, we observe a steeper slope in the log-linear relationship than observed empirically.

DISTRIBUTION A: Distribution approved for public release.

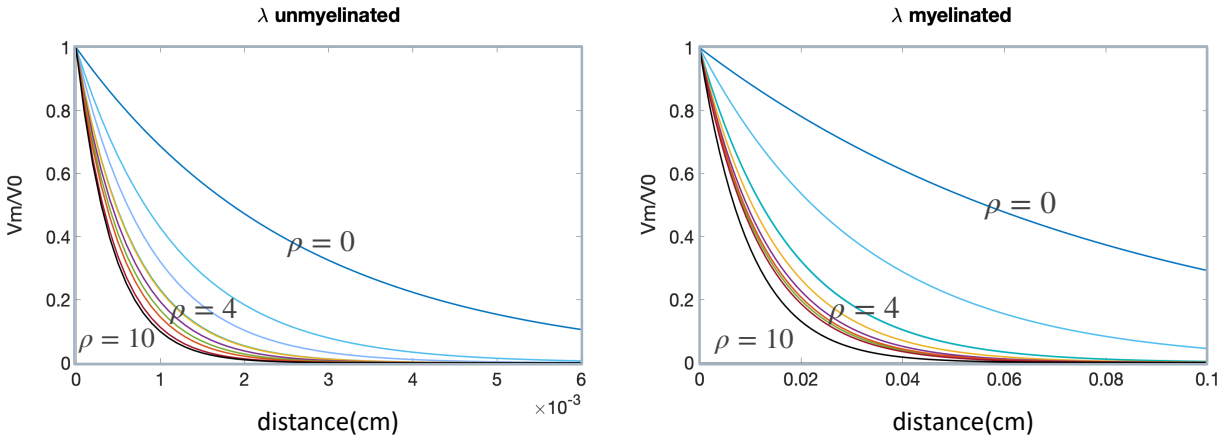


Figure 10: Plot of the distribution of membrane potential along the axon as a fraction of the initial maximum voltage V_0, for space constant $\boldsymbol{\lambda}$ values calculated across a range of resistivity ratios $\boldsymbol{\rho}$ for unmyelinated (left) and myelinated neurons (right).

IV. Conclusions & Discussion

Ephaptic coupling was first described in the 1940s, yet the possibility that nearby axonal signaling can alter the velocity or synchrony of spikes traveling in brain white matter is surprisingly understudied. Recently, a few computational studies have examined ephaptic coupling in white matter fascicles e.g., (Sheheitli and Jirsa 2020); (Schmidt, Hahn et al. 2021). These studies reported a slowing of spike propagation velocity that paralleled increased ephaptic strength, and spike synchronization with specific ephaptic strengths. Our model is consistent with these studies, where a nonlinear relationship was observed between coupling strength, axonal caliber, and velocity.

To our knowledge, this is the first computational study to explore the relationship between ephaptic coupling in white matter fiber bundles and 1/f spectra observed in EEG/MEG data. Our model generated spike velocity estimates, and thus signal transmission latencies using morphometric properties derived from dMRI data. Within a recursive signaling framework, our model was then capable of generating spectral decompositions across a range of ephaptic coupling values.

In the present work, our computational model assumed that nodes of Ranvier were evenly spaced along the axon, and did not consider nodal alignment. Previous studies in peripheral neurons have demonstrated that alignment or lack thereof has negligible effect on spike velocity and space constants (Neishabouri and Faisal 2014).

Neurons in human white matter appear to be distributed randomly, as opposed to with stereotyped patterns observed in other species (e.g., rabbit) (Waxman and Swadlow 1977). Understanding how this random distribution gives rise to the high packing density observed in human white matter may be the focus of mathematical modeling of neural arrangements,

DISTRIBUTION A: Distribution approved for public release.

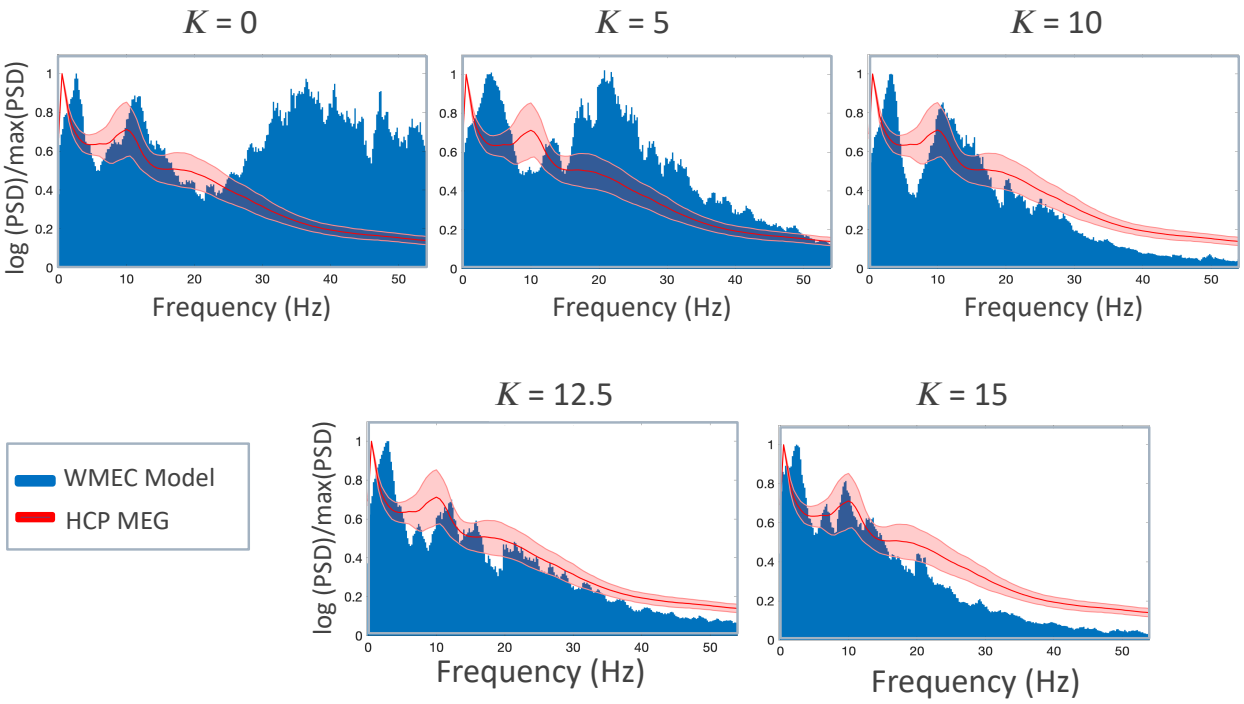


Figure 11: Spectral densities generated by the white matter ephaptic coupling model (blue), with the empirical MEG spectral distribution computed across the HCP data set with mean and standard deviation shown in red. When the ephaptic coupling was set to zero (top left), the higher frequencies in the beta and gamma frequency contribute strongly to the spectral distribution, and do not follow a log-linear 1/f relationship. Ephaptic coupling at a strength of 10 began to show log-linear characteristics (top right). A kappa of 12.5 had the maximum cross-correlation with the empirical MEG distribution. At a kappa of 15, there is a diminution in the higher frequency power, though the "alpha peak" appears to be correlate with the empirical data. Note that each run of this model requires ~1000 hours of computing time.

potentially using 'fuzzy solutions' to the circle packing problem to create more biologically plausible geometries of myelinated and unmyelinated neurons within the white matter fibre bundle.

In our model, we used parameters from (Braitenberg and Schuz 2002) to model short association or U-fibers. In this study, U-fibers were reported to account for 90% of total white matter volume with fiber lengths ranging from 3mm to 30mm. A recent dMRI study at 7T, characterized fine detail of U-fibers, and reported lengths up to 45 mm, though only a small subset of U-fibers in visual cortex were studied (Movahedian Attar, Kirilina et al. 2020). This paper reported reduced volume in the longer U-fiber (> 30 mm) tracts. Interestingly, the myelination of U-fiber tracts continues to mature into late adulthood. Therefore, future work may explore how varying the ratio of myelinated axons as a function of age effects predicted spectral densities. Future work

DISTRIBUTION A: Distribution approved for public release.

may also explore optimizing this model further by including further anatomic details from high resolution tractography imaging (McColgan, Helbling et al. 2021).

Supplementary Table 1: White Matter Geometric Properties derived from HCP dMRI data
Mean Tract Length [Length(mm)] and Mean Volume (mm3) are show with corresponding standard deviation (SD) for each white mater tract

Tract	Length (mm)	SD	Volume (mm^3)	SD
Left Cingulum Parahippocampal	45.41	2.52	4182.2	875.79
Right Cingulum Parahippocampal	47.57	2.31	5050.4	1030.2
Right Vertical Occipital Fasciculus	49.87	2.87	8334.3	1609.1
Left Vertical Occipital Fasciculus	51.57	2.72	32093	9932.2
Right Corticopontine Tract Parietal	61.83	22.83	7373.1	1333.8
Left Corticopontine Tract Parietal	64.38	24.82	33627	9402.3
Right Uncinate Fasciculus	62.39	8.42	27147	7852.5
Left Uncinate Fasciculus	64.47	7.42	26690	6886.8
Right Thalamic Radiation Superior	66.47	4.81	8485.4	10359
Left Thalamic Radiation Superior	69.41	6.00	10777	7501.9
Left Cingulum Parahippocampal Parietal	72.70	7.38	14454	4185.5
Right Thalamic Radiation Posterior	74.61	6.13	19226	3035.7
Left Thalamic Radiation Posterior	76.33	6.35	30316	6681.5
Right Thalamic Radiation Anterior	78.07	6.95	11740	4462.2
Left Thalamic Radiation Anterior	79.41	6.17	8463.7	5053.9
Right Superior Longitudinal Fasciculus3	80.33	5.23	16273	3441.2
Left Superior Longitudinal Fasciculus3	80.16	3.77	27450	6659.8
Right Superior Longitudinal Fasciculus2	84.10	9.56	29415	4408.3
Left Superior Longitudinal Fasciculus2	82.90	4.10	21620	4216.3
Right Superior Longitudinal Fasciculus1	84.86	5.28	22359	4870.8
Left Superior Longitudinal_Fasciculus1	85.87	5.36	4340.3	3579.6

DISTRIBUTION A: Distribution approved for public release.

Right Reticulospinal Tract	92.60	18.40	6549.4	5933.5
Left Reticulospinal Tract	93.74	18.44	19244	3925.3
Right Parietal Aslant Tract	86.09	6.58	13733	3274.5
Left Parietal Aslant Tract	86.93	7.38	13842	2489.8
Right Optic Radiation	92.31	6.00	20849	5677.8
Left Optic Radiation	93.40	6.74	19622	4579.3
Right Middle Longitudinal Fasciculus	93.48	5.14	4683.3	2182
Left Middle Longitudinal Fasciculus	95.25	7.61	28756	9064.3
Right Medial Lemniscus	98.80	13.96	19998	4397.9
Left Medial Lemniscus	100.07	14.20	19759	3838
Right Inferior Longitudinal Fasciculus	100.13	10.14	16383	9053
Left Inferior Longitudinal Fasciculus	101.42	9.58	10689	8135.2
Right Inferior Fronto Occipital Fasciculus	108.97	25.42	22283	9229.8
Left Inferior Fronto Occipital Fasciculus	110.87	26.60	12710	9040.8
Right Frontal Aslant Tract	99.74	9.24	21187	3534.5
Left Frontal Aslant Tract	101.30	8.72	14296	4783.7
Right Fornix	103.83	6.63	7446.1	1740
Left Fornix	104.83	8.26	8945	2697.9
Right Extreme Capsule	108.72	5.15	10320	2318.6
Left Extreme Capsule	110.75	5.50	7449.2	1483.8
Right Dentatorubrothalamic Tract	115.88	7.83	43797	9273.3
Left Dentatorubrothalamic Tract	117.86	8.02	15589	2289.4
Right Corticostriatal Tract Superior	111.22	18.12	10851	9849.4
Left Corticostriatal Tract Superior	112.60	18.94	95081	23847
Right Corticostriatal Tract Posterior	117.29	9.68	10595	4707.4
Left Corticostriatal Tract Posterior	118.64	9.44	8991.4	4763.7
Right Corticostriatal Tract Anterior	114.85	21.85	11888	7147.2
Left Corticostriatal Tract Anterior	115.99	21.90	12709	7095.7
Right Corticospinal Tract	124.99	5.32	11140	1555
Left Corticospinal Tract	125.93	5.20	21575	3967.4
Right Corticopontine Tract Occipital	126.57	4.98	28527	6609.8

DISTRIBUTION A: Distribution approved for public release.

Left Corticopontine Tract Occipital	128.04	6.11	35103	9834.1
Right Corticopontine Tract Frontal	127.43	4.99	9280.2	3764.4
Left Corticopontine_Tract Frontal	127.95	5.49	28244	6304
Right Corticobulbar Tract	128.72	4.96	18067	4366.2
Left Corticobulbar Tract	129.59	5.05	14803	4672.7
Corpus Callosum Tapetum	134.36	13.16	13085	2218.5
Corpus Callosum Forceps Minor	129.46	8.09	21187	10614
Corpus Callosum Forceps Major	136.80	12.15	11696	11808
Corpus Callosum Body	132.04	6.99	20265	30502
Right Cingulum Rarolfactory	134.02	5.99	7400.8	1649.3
Left Cingulum Rarolfactory	130.48	18.12	8557.5	2649.8
Right Cingulum Parahippocampal Parietal	132.55	17.32	19365	5228.4
Right Cingulum Frontal Parietal	137.24	11.32	14607	4362.6
Left Cingulum Frontal Parietal	142.63	12.04	25488	4540.2
Right Cingulum Frontal Parahippocampal	150.26	17.19	10684	1906.3
Left Cingulum Frontal Parahippocampal	159.93	16.30	15316	4807.1
Right Arcuate Fasciculus	168.93	16.52	39248	10943
Left Arcuate Fasciculus	175.16	29.86	36632	5793.9
Anterior Commissure	198.21	31.50	33873	5744
Right Acoustic Radiation	183.60	45.29	1552.2	387.62
Left Acoustic Radiation	153.80	88.01	1392.7	455.69

DISTRIBUTION A: Distribution approved for public release.

OBJECTIVE 2: Empirically test theory in humans using transcranial ultrasound (TUS)

Abstract:

The alpha rhythm is perhaps the most prominent feature in EEG recordings, yet its spatial origins and functional significance have been debated since its was first observed in 1929. The alpha rhythm evolves over the lifespan, and first emerges around the second year of life. Because changes in myelination appear to parallel the emergence and of power of this rhythm, we hypothesized that white matter signaling may play a role in generating the alpha rhythm. To explore this theory, we applied transcranial ultrasound (TUS) sonication to healthy adult subjects in the following brain regions: corpus callosum, u-fiber tracts, medial dorsal thalamus, and the pulvinar nucleus. EEG was recorded while subjects performed an eyes open/eyes closed task. We found no significant alpha power changes following TUS to any gray matter region. In contrast, we observed a significant diminution in alpha power following TUS applied to the corpus callosum. Our results suggest that the corpus callosum is either responsible for, or is an integral component requisite for the generation of the alpha rhythm in human EEG recordings.

I. Introduction

In Berger's pioneering work, he noted prominent "alpha waves" that were abolished with the eyes open in the first recorded human EEG (Berger 1929); (Stone and Hughes 2013). For some years thereafter, it was referred to as the Berger rhythm, and its was suggested that these waves were generated in occipital regions reflecting an "idle state" (Adrian and Matthews 1934). In 1977, electrode recordings in laminar layers IV and V of dog cortex suggested that the alpha rhythm was centered in the visual cortex (Lopes Da Silva and Storm Van Leeuwen 1977). Combined cortical surface, intracortical depth electrode, and intra-thalamic recordings provided additional evidence that alpha may be generated by pyramidal neurons in visual cortex, and that the pulvinar nucleus and other nuclei of the thalamus influence cortical alpha activity (Lopes da Silva 1991).

The alpha rhythm is also a conspicuous signature in sensory motor regions. The "rolandic mu-alpha rhythm" appears during rest and diminishes during movement with a slightly higher frequency than alpha rhythms of the visual cortex. These two alpha signatures have no significant coherence, and are therefore often thought to be distinct (Lopes da Silva 2023). Alpha desynchronization in specific regions occurs as attention is focused on particular information e.g., (Klimesch, Sauseng et al. 2007), and may help shape inhibitory control and other executive functions. Thus, the functional significance of the alpha rhythm is varied and its distribution has has been linked to the lateral geniculate nucleus, pulvinar, and thalami-cortical activity, and pyramidal cells in visual and sensory motor regions

However, additional clues as to the origin of alpha rhythms can be found in brain development. During infancy, white matter microstructure matures rapidly, causing changes in axon caliber, myelin content, and fiber packing density (Krogsrud, Fjell et al. 2016). White matter tracts are

DISTRIBUTION A: Distribution approved for public release.

difficult to distinguish from gray matter on MRI images collected during the first 6 months of life (Mostapha and Styner 2019).

Similarly, at birth and throughout infancy, there is no distinguishable EEG alpha rhythm (Trujillo, Gao et al. 2019). Throughout early development, the slope of the log-linear 1/f increases (Schaworonkow and Voytek 2021), and alpha power continues to evolve over the lifespan (Voytek, Kramer et al. 2015) (Figure 12). Given that the emergence of the alpha rhythm appears to parallel the development of myelin and the formation of white matter fiber bundles, we hypothesized that white matter tracts may either be responsible for the generation of this signal, or alternatively are a requirement for emergence of alpha signals.

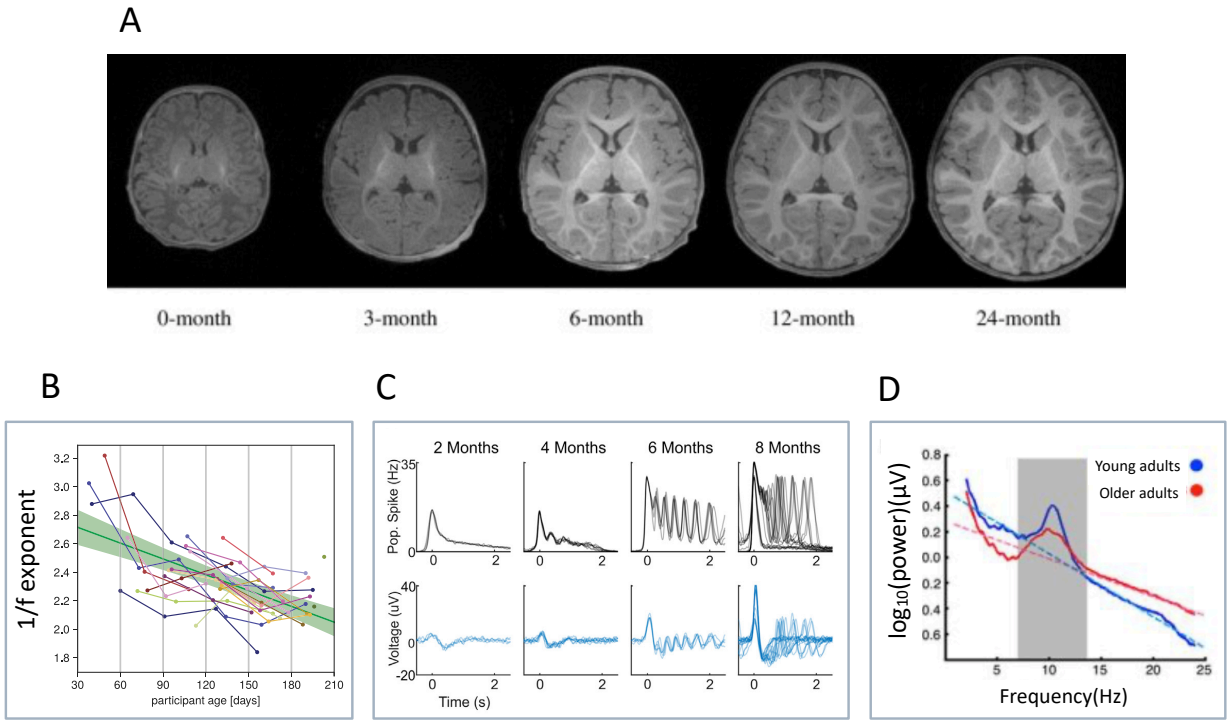


Figure 12: **A**) T1 weighted structural MRI over the first two years of life. At birth, white matter tracts are not present. At 6 months, white matter tracts begin to form, and by two years of life, there is a strong contrast between gray matter and white matter tracts. (Mostapfa & Styner (2019) **B**) The exponent that characterizes the log-linear EEG spectra is altered over the course of development (Schawarenkow & Voytek (2021). **C**) The alpha rhythm begins to emerge in infant around 8 months (Trujilo et al. 2019). **D**) The alpha rhythm continues to change from early too later adulthood (Voytek et al. 2015)

To explore this theory, we leveraged a novel brain stimulation technique, transcranial ultrasound (TUS), to test which whether alpha was altered during sonication of the putative alpha generators in thalamus and cortical regions. We then examined whether modulation of spikes traveling along white matter fiber bundles altered alpha power measured in scalp EEG.

DISTRIBUTION A: Distribution approved for public release.

Transcranial Ultrasound

Ultrasound is traditionally known for its visualization properties - providing images of a child before birth. However, the lesser-known ability of these high-frequency sound waves to alter brain activity has also been studied almost continuously since the 1950s e.g., (Fry 1958). When pulsed at *high* intensity (HIFUP), the thermal effects of ultrasound are significant, and this property can be leveraged for selective ablation of deep brain structures, obviating the need to cut through intervening brain tissue. Although useful for certain surgical techniques, high intensity ultrasound is not suitable for human brain research (for review, see (Bystritsky, Korb et al. 2011). When pulsed at low intensity, the thermal effects of transcranial ultrasound (TUS) are negligible e.g., (Bushberg, Seibert et al. 2021). After numerous safety studies, the FDA approved TUS devices in 2014, and the current safety limits are well below the threshold for thermal effects.

Given the novelty of this experimental modality, the cellular mechanisms of action have not been fully elucidated. At low intensity, thermal effects are negligible. Therefore, there are two alternative effects that may subtend TUS neuromodulation. The first is cavitation. Cavitation occurs when ultrasound waves of sufficient intensity resonate, expand, and collapse gas bubbles within tissue. Cavitation is fundamentally a mechanical effect that creates stable oscillations of gas bubbles at multiple frequencies. Although micro-cavitation can induce alterations in lipid bilayer capacitance, the effects of cavitation are thought to be small when delivered within the range of currently approved sonication limits (Bystritsky, Korb et al. 2011).

Electrophysiological-mechanical coupling is thought to be responsible for the majority of excitation and suppression observed in human research. Neurons have a low elastic modulus and are therefore considered viscoelastic. In this sense, neurons have the capability of propagating mechanical energy *elastically* as cells are deformed. These elastic properties allow for

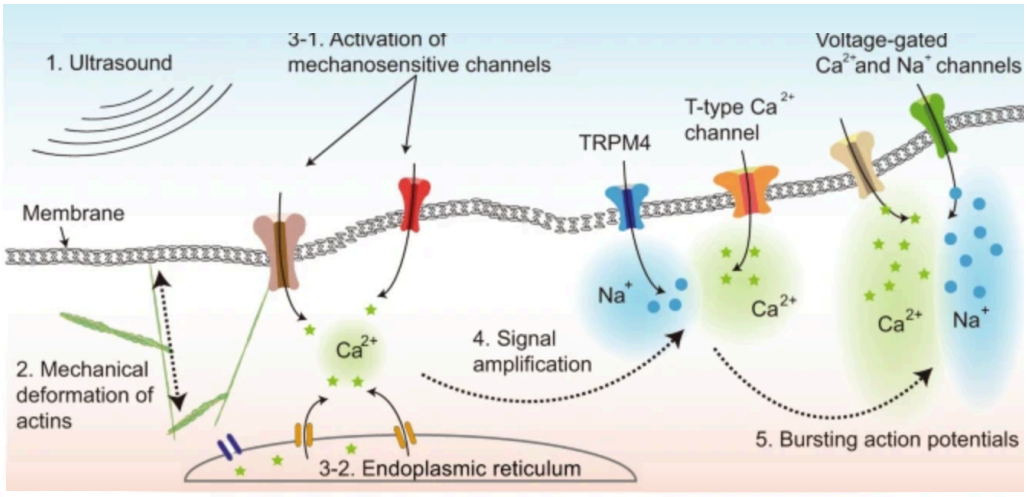


Figure 13: The bioacoustic effects of ultrasound appear to b mediated by calcium-selective mechanosensitive ion channels, and amplified via calcium and voltage-gate ion channel, with converging evidence from pharmacological and genetic inhibition of these ion channels (Yoo et al. 2022).

DISTRIBUTION A: Distribution approved for public release.

mechanical interactions in the neuron's cytoskeleton, cell adhesion molecules, and can alter the probability of ion channel gating. The mechanical energy is therefore translated into different conformational states, resulting in pressure-induced voltage changes in the intracellular and extracellular milieu *for review*, see (Dell'Italia, Sanguinetti et al. 2022).

Recent genetic knockout and ion channel blocker studies have demonstrated that numerous mechanosensitive ion channels are expressed at the neuronal membrane, that seem to mediate TUS effects through calcium signaling (Yoo, Mittelstein et al. 2022), Figure 13). Notably, resonance in microtubules localized primarily to myelinated axons has also been studied, and the complex cellular signaling pathways altered by TUS in white matter are thought to produce substantial effects e.g., (Oh, Lee et al. 2019). The biophysics of TUS effects at the cellular level remains an active area of research.

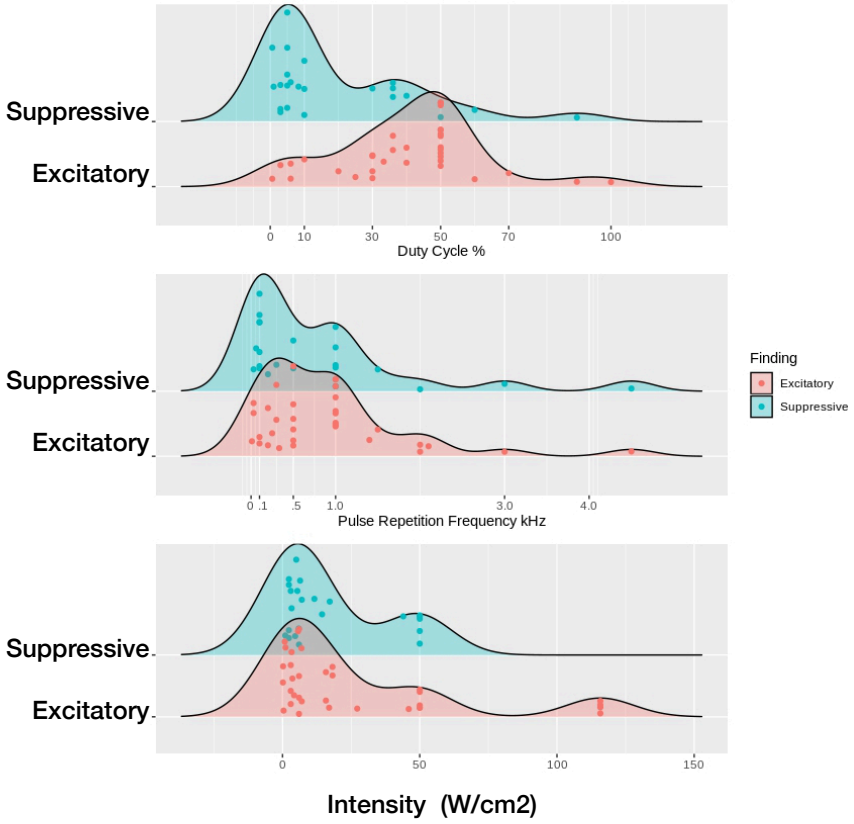


Figure 14: The acoustic envelope, a measure of intensity, duty cycle, and pulse repetition frequency, predicts the magnitude and type of effect (suppression or excitation) observed following transcranial ultrasound sonication (TUS) (D'Italia et al. 2022)

Ultrasound waves occupy a broad range of frequencies (100kHz-100MHz). These ultrasonic waves can propagate in two ways: longitudinally and transversely. Transverse waves vibrate perpendicularly to the direction of wave energy, but are only present in solids (e.g., bone). In

DISTRIBUTION A: Distribution approved for public release.

soft brain tissue, we are concerned with longitudinal waves. Acoustic waves have characteristic properties, similar to any other wave, including wavelength, frequency, and amplitude.

Frequency is particularly relevant to brain stimulation because the focal point of the acoustic waves is where the effects are exerted, and hence why TUS does not alter activity in intervening tissue. The spatial extent of TUS effects are *inversely* proportional to the frequency. When pulsed, both the duty cycle and pulse repetition frequency become important parameters. The duty cycle ratio represents the percentage of time that the sonication is 'on.' In our preliminary experiments, we have noted that when duty cycle is set to 100%, we observe no effects of TUS. At approximately, 50% duty cycle, the excitatory effects seem to dominate, while lower duty cycles appear to create suppressive effects (Figure 14). When synthesizing our experimental data, it appears as though the acoustic envelope may determine the extent and type of the TUS effect.

Given that activity in pulvinar nucleus modulates cortical alpha, we included this site as a brain stimulation target. Because the alpha power is diminished during eyes open states compared to eyes closed, we tested whether modulation of activity in the lateral geniculate nucleus (LGN), which projects to visual cortex, would modulate EEG alpha. For white matter tracts, we targeted short association U-fiber tracts, and the large corpus callosum white matter tract. As a control condition, we sonicated the vasculature superior to the corpus callosum at the midline.

II. Methods

All study protocols were approved by the CCN IRB prior to commencing studies. Individuals with metal implants, psychiatric or neurologic disorders such as epilepsy, structural brain abnormalities, or individuals who might be pregnant were excluded from participation. All subjects were permitted adequate time to review all protocols. Informed consent was obtained prior to commencing protocols for this study. All subjects received TUS sonication at a single site during a given session. A total of 24 subjects were enrolled in the study. A subset of subjects (N=8) returned on a different day to receive sonication at a different brain target. Thus, there were a total of 30 data collection sessions across the study cohort (mean age = 19 +/- 6 y.o., 33% female). An overview of our neuroimaging, EEG and brain stimulation protocols is shown in Figure 15.

Magnetic Resonance Imaging

All subjects were scanned on a Siemens 3 Tesla Prima scanner using a 32 channel head coil. Arteriole Spin Labeling MRI scans are uniquely altered in response to TUS. Thus, ASL MRI was collected for baseline, sham, and test conditions, using the following parameters: slice thickness 3 mm, field of view (FOV) 192 mm, a TR of 4600 ms, TE of 16.18 ms, using an interleaved multi-slice mode imaging. Resting state fMRI was collected for 6 minutes using a 2.0 mm isotropic voxel size, TR of 800 ms, TE of 37 ms, with a multi band acceleration factor of 8. High resolution T1 imaging was performed with 0.8 mm isotropic voxel size, 2500ms TR, 2.22 ms TE, and 8 degree flip angle. Diffusion MRI was required for inputs into our computational model. Diffusion MRI was collected at 1.5 mm isotropic voxel size using a 3230 ms TR, 89.2 ms TE, using an interleaved sequence with a multi-band acceleration of 4. MRI scanning was

DISTRIBUTION A: Distribution approved for public release.

done prior to any EEG/TUS work to control for the possibility that MR alters any other procedures. ASL and rs-fMRI scans were repeated after each TUS-EEG conditions.

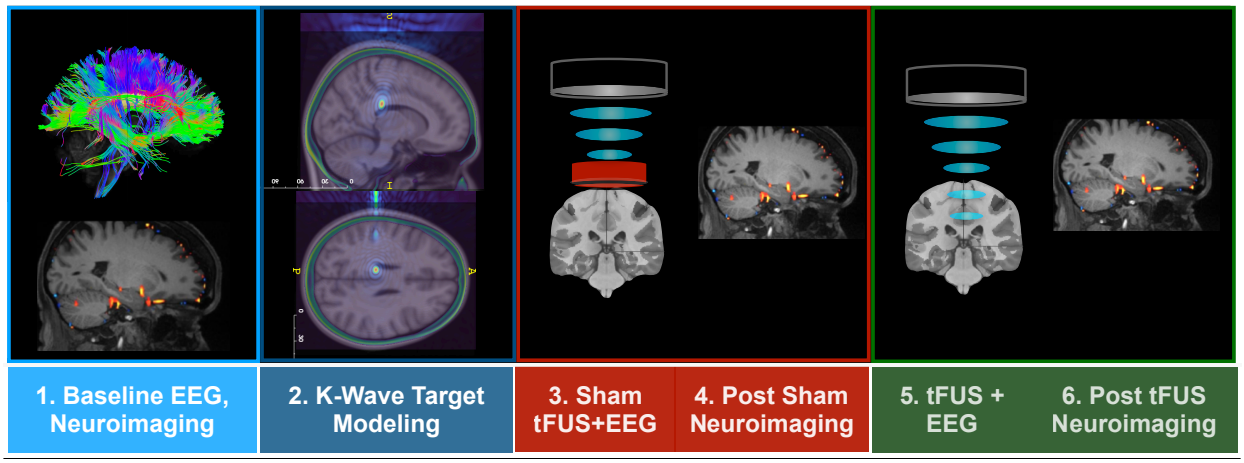


Figure 15: Overview of experimental protocols. (From left to right) Baseline measurements included: resting state fMRI, arteriole spin labeling (ASL), diffusion MRI (dMRI), MPRAGE T1 MRI, and task EEG recordings for eyes open/ eyes closed, motor finger tapping, and an adapted novelty odd-ball paradigm. The following sham TUS experiment included repeating all EEG tasks, and collecting ASL MRI imaging. Finally, the TUS sonication was applied, and subjects repeated EEG tasks. A final ASL MRI scan was repeated to localize the effects of TUS sonication.

EEG Recordings

All EEG data were collected in a copper shielded room at the CCN using a modified high density EEG sensor net. EEG was either recorded using a modified 256 electrode Magstim EGI Electrical Geodesic EEG cap (10 sessions) or a modified Brain Products 64 channel Acticap (24 sessions) at a 5000 Hz sampling rate. EEG sensor nets were modified to remove electrodes to accommodate bioacoustic coupling of the ultrasound transducer, and data acquisition during and immediately following sonication. Modified electrode montages are shown in (Figure 16 a, b).

EEG Behavioral Paradigms

The PI developed Psychtoolbox code to present stimuli to participants during EEG data acquisition. We selected three behavioural tasks known to produce characteristic responses in EEG across spectral frequencies, and evoked potentials (Figure 16).

In the first task, we used the classic eyes-open / eyes-closed (EOEC) experimental paradigm, known to produce robust alpha power diminution during the eyes open condition (e.g., Goldman et al. 2002). This task consisted of 3 blocks of eyes open/eyes closed for 30 seconds each to permit time for changes in the alpha power. In the second task, participants performed cued left and right *finger tapping* movements for 30 seconds each followed by a rest condition for 2 blocks. This task was chosen because figure tapping produces robust alterations in the mu-alpha and beta frequency bands, evident in both ipsilateral and contralateral EEG channels.

DISTRIBUTION A: Distribution approved for public release.

Lastly, subjects performed a modified oddball stimulus paradigm that included standard tones, oddball tones, and novel sounds. We used a sound library kindly shared by Robert Barry (AUS). In many oddball paradigms, the subject's response time to hearing an oddball sound is recorded. We had subjects listen passively to sounds avoid any additional changes in EEG due to button-press movement. The oddball paradigm creates robust changes in the P300 evoked EEG response, and is thought to reflect the orienting response due to attentional shifting. The novelty oddball task paradigm consisted of subjects listening to standard tones at 1000Hz (probability 0.8), oddball tones at 2000 Hz (probability 0.1), and novel sounds (probability 0.1) for a total of 480 trials. Stimuli were randomized and jittered with a minimum inter-stimulus interval of 2 sec.

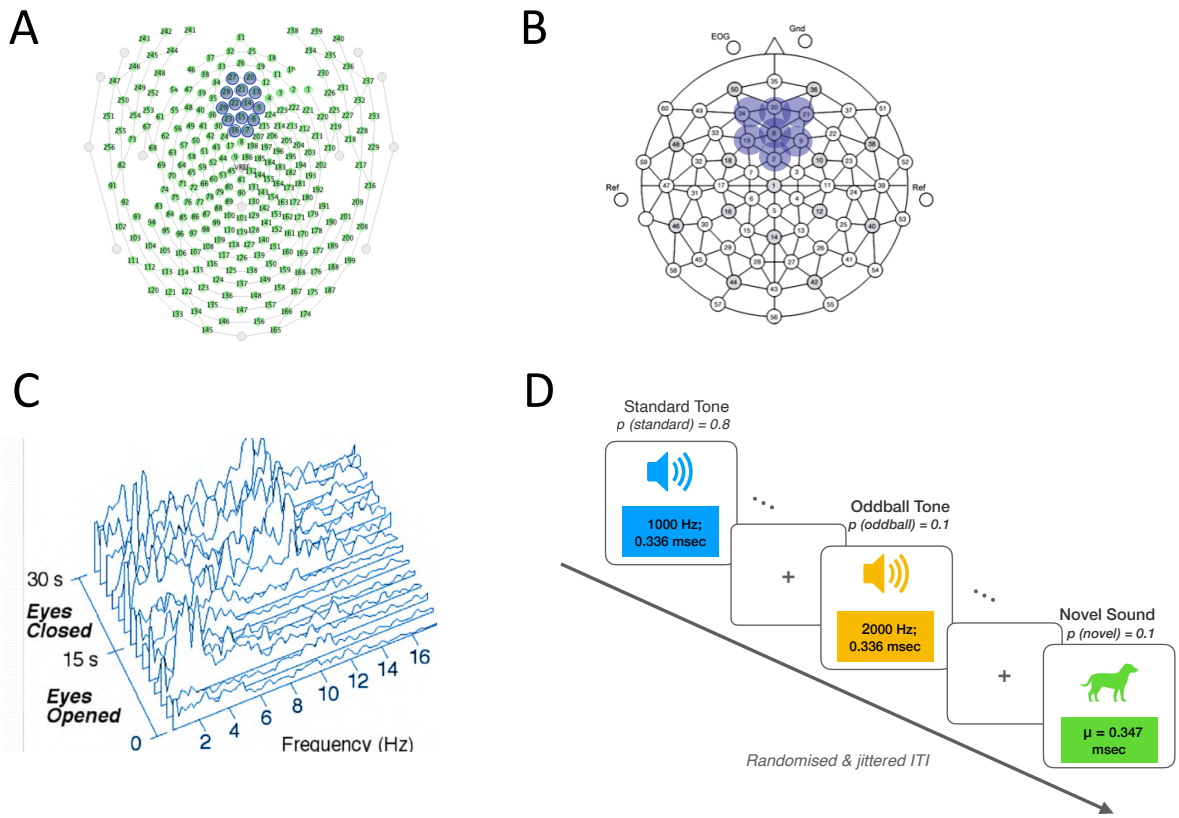


Figure 16: A) The channel montage for our modified 256 electrode EEG Magstim EGI electrical geodesic cap. The shaded channels (blue) indicate electrodes that were removed from the net to accommodate bioelectric acoustic coupling. B) Channel montage, similar to A, but for the BrainVision Acticap EEG net. C) Robust alpha power desynchronization that takes place over the course of the eyes-open/eyes-closed task (Goldman et al. 2002). D) The novelty oddball task paradigm consisted of subjects listening to standard tones at 1000Hz (probability 0.8), oddball tones at 2000 Hz (probability 0.1), and novel sounds (probability 0.1) for a total of 480 trials.

DISTRIBUTION A: Distribution approved for public release.

Transcranial Ultrasound Sonication Procedures

The Brainsonix BX Pulsar device was used to deliver all ultrasound sonication across all brain targets for sham and test conditions. We used a 650 kHz frequency for sonication with a pulse repetition frequency of 10Hz, and a 0.05 duty factor. Sonication duration took place for 30 seconds on, and 30 seconds off for a total of 10 minute. Transducer depths (35, 55, or 65mm) were selected based on the desired target, and measurements obtained using the high resolution MPRAGE T1 MRI scan using software available on the Tim Trio scanner. Stand-off pads of appropriate depth were used as necessary to accommodate individual anatomy, and localization of the acoustic foci.

During the baseline condition, EEG data was collected and no sonication was applied. However, the BX Pulsar device was turned on during this experiment to avoid a potential auditory confound related to instrumentation noise. During the "sham" condition, the TUS sonication was applied with the aforementioned parameters, but a sham "stand-off" pad was placed between the ultrasound transducer and the scalp. These sham stand-off pads block ultrasound wave. This was done to control for the possibility that the auditory evoked potentials or other EEG signatures were altered due to instrumentation noise from the ultrasound machine. This blocker material provides an important control condition to rule out this possibility

Brain Targets for Sonication

Subjects were randomly assigned to receive sonication in one of five different locations. These loci were chosen carefully to test our hypothesis, specifically that sonication of white matter would alter 1/f spectral densities

Corpus Callosum

For our first brain target we applied suppressive TUS to the A/P midpoint crossing of CC crossing fibers. This was selected for 2 reasons. 1) Our model predicts that the CC generates the alpha rhythm. 2)The CC is large and accessible to TUS, and the acoustic focus is not expected to target other brain regions at this point (based on k-wave modeling). Furthermore, if EEG is only generated by superficial gray matter (according to traditional theory), then suppressing a a deep brain target have minimal effect on measured signals. This provided the opportunity for us to empirically test our alternate theory - that EEG/MEG spectral rhythms are generated by WM.

Vasculature Superior to CC (Negative Control Condition)

To control for the possibility that TUS is exerting its influence via changes in the vasculature superior to the corpus callosum, our second point selected was a region just superior to the CC. This also helps rule out the possibility that brain activity is altered via suppression at the edges of the acoustic focus.

U-fibers (gamma rhythm)

DISTRIBUTION A: Distribution approved for public release.

Superficial U-fiber crossings were selected for two key reasons. First, our model predicts that U-fibers generate gamma rhythms, offering the opportunity to test an additional brain rhythm mapping. Second, these fibers are easily accessible via TUS applied at the pterion - the thinnest portion of the scalp. Specialized shallow depth transducers were developed by Mark Schaffer at Brainsonix for the PI, specifically for this project.

Thalamic Nuclei (Pulvinar Nucleus, Dorso-medial thalamus)

In order to test whether sonication of deep gray matter nuclei would induce measurable changes in EEG, a subset of subjects received sonication at either the pulvinar nucleus or dorso-medial region of the thalamus. Given that pulvinar nucleus and thalamo-cortical activity have been suggested as putative generators of the alpha rhythm, these areas were selected as brain targets in this experiment.

Statistical Analysis

EEG Recordings

All EEG data analysis was performed using EEGLAB v.2020.0 with Matlab R2023a. EEG data preprocessing included running a first-order high pass filter, removal of channels that were not included in the montage, and eye blink artifact removal. Thereafter, spherical interpolation of missing channels was applied and EEG data was segmented according to event markers. For the EO/EC task, data was segmented into 10 sec windows that included 5sec before and 5sec after eyes open. Data from the motor task was also segmented into 10 sec windows, with 5 sec before and after initiation of finger tapping cue.

Spectral decompositions were calculated for each segmented event for a 2 sec time window that began 3 sec prior to either the eyes open or finger tapping cue for tasks 1 and 2 respectively. A second spectral decomposition was performed on a 2 second window beginning 2 seconds after either the eyes open or finger tapping cue to allow time for changes in alpha power. From each of these spectral decompositions, the peak alpha value or maximum value of the power spectral density between 8-12 Hz was extracted. Given variability amongst individuals in the peak alpha magnitude and spectral position, we computed relative change in peak alpha for each event across baseline, sham and TUS conditions. Wavelet decomposition were performed on each of these segments for all subjects for time-frequency analysis.

Magnetic Resonance Imaging

Structural and functional MRI data were analyze with FSL (https://fsl.fmrib.ox.ac.uk/fsl/fslwiki/). All functional data underwent brain extraction and registration to MNI space. Resting-state function MRI and Arteriole Spin Labeling (ASL) data also underwent high pass filtering and motion correction. All ASL data underwent general linear modeling (GLM) analysis using FSL FEAT. Contrasts for this analysis included baseline-sham, sham-baseline, baseline-TUS, and TUS-baseline.

III. Results

DISTRIBUTION A: Distribution approved for public release.

During both baseline and "sham-TUS" EEG recordings, we observed a prominent alpha peak in spectral decompositions across participants during the eyes closed. We see no signifiant change in alpha power between baseline or sham conditions. Thus, the sham stand-off pad appears to be effective at attenuating the ultrasound. This was also evident in materials testing experiments from our colleagues at Brainsonix.

Spectral decompositions and wavelet (time-frequency) decompositions also show no significant changes during the actual TUS condition for *gray matter* targets including the Pulvinar nucleus and the Medial Dorsal nucleus of the thalamus. Interestingly, a prominent alpha desynchronization is observed following suppressive TUS to corpus callosum (Figure 17), but not when suppressive TUS is applied to U-fiber crossings, superficial motor cortex, or deep cortical nuclei.

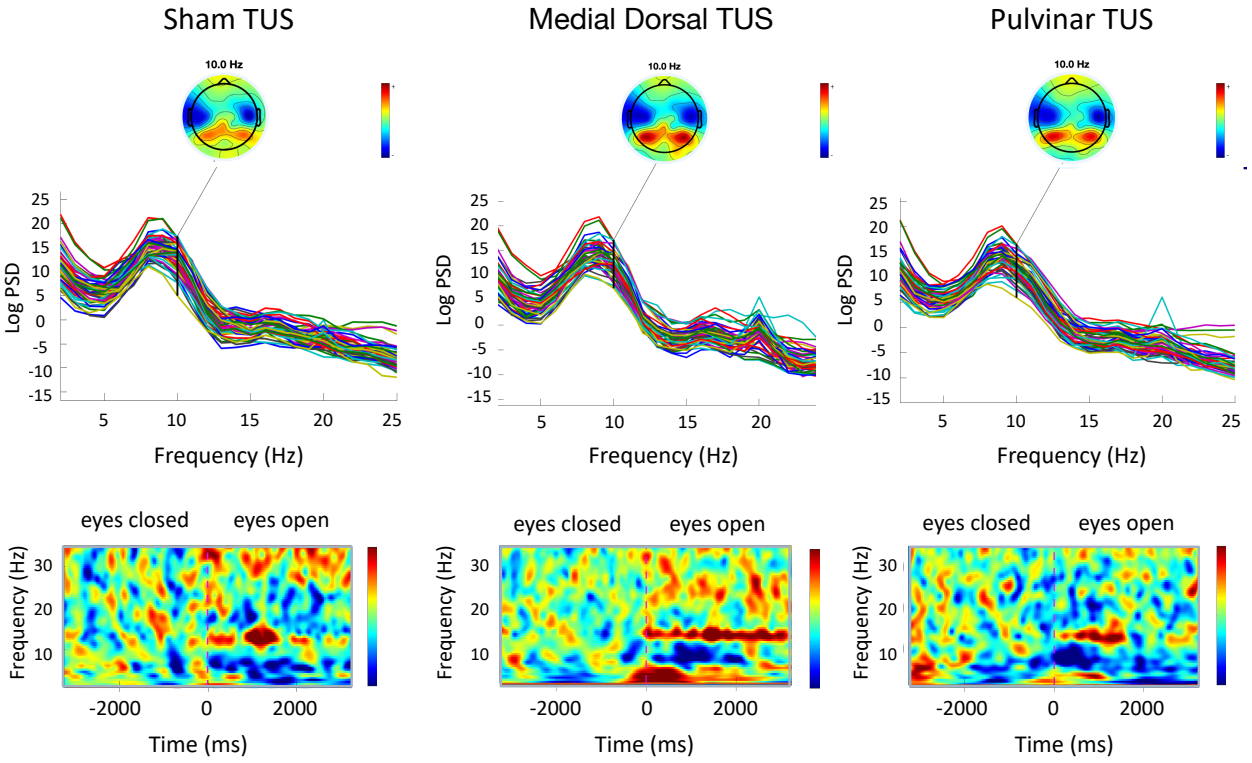


Figure 17: (Top) Spectral decompositions calculated for 2 seconds of eyes closed data for sham-TUS (left), medial dorsal nucleus (middle), and pulvinar nucleus (right) from the occipital EEG channel. Suppressive TUS at 650kHz, was applied using a 10Hz envelope for 10 minutes prior to the eyes open/eyes closed task. In the case of the sham condition, the stand-off pad was placed between the transducer and the scalp to block ultrasound waves, while permitting instrumentation noise to alter brain activity. (Lower) Wavelet decompositions from occipital channels for sham, medial dorsal, and pulvinar nucleus show clear diminution in the alpha power during the eyes open condition.

DISTRIBUTION A: Distribution approved for public release.

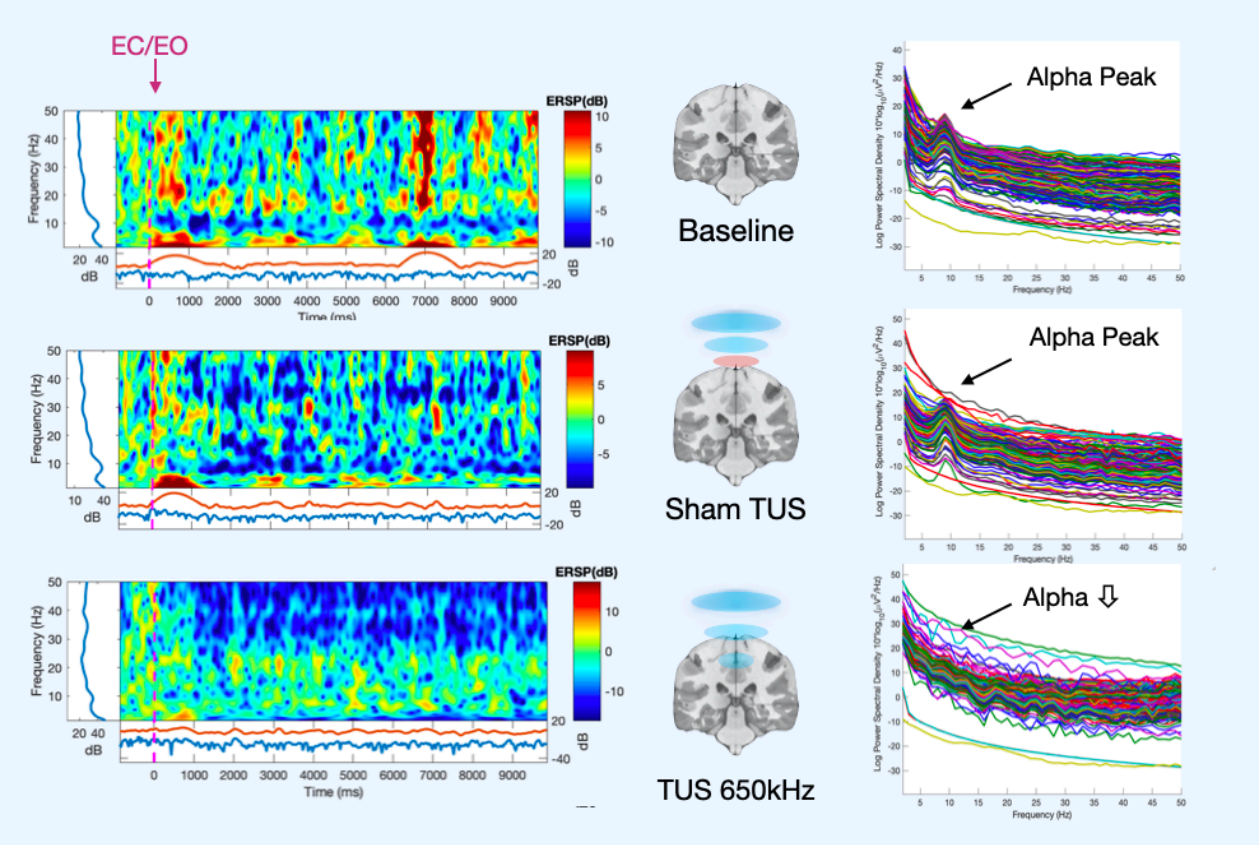


Figure 18: Alpha Power Desynchronization following Suppressive TUS to Corpus Callosum midline crossings in a representative subject. (Left) Time-frequency decompositions for 1 second before and 10 sec after the subject transitioned from eyes closed to eyes open for baseline (top), sham-TUS (middle), and TUS sonication (lower). (Right) Special decompositions calculated from 2 seconds of eyes closed EEG data for baseline, sham, and TUS (top, middle, lower panels, respectively). At baseline, a prominent alpha peak is observed during the eyes closed condition. This peak is also evident during sonication with a sham stand-off pad, controlling for signal noise. TUS at 650kHz, was applied with a 10Hz envelope, using the same sonication parameters as Figure 17.

In contrast, we observed a prominent diminution in alpha power following suppressive TUS to corpus callosum (Figure 18). This alpha power diminution is evident across both spectral and wavelet (time-frequency) decompositions.

DISTRIBUTION A: Distribution approved for public release.

IV. Discussion & Ongoing Analysis

Here, we applied TUS in a novel capacity, to study the effects of ultrasound on the EEG alpha rhythm. To our knowledge, there is only one other study combining EEG and TUS in humans. This study reported changes in evoked potentials following TUS administration (Lee, Kim et al. 2016). It is possible that their TUS device may have created an auditory confound, given that this study failed to use an appropriate sham condition. In our study, we leveraged novel stand-off pads to control for this possibility, and found no significant difference between baseline measurements and sham-TUS.

Suppressive TUS applied to gray matter targets, the medial dorsal and pulvinar nuclei, did not significantly alter alpha power during the eyes closed state, when the alpha peak is conspicuous. The frequency position of the alpha peak also remained unchanged when TUS was applied to gray matter targets.

In contrast, suppressive TUS applied to corpus callosum caused a prominent desynchronization in alpha power during the idle eyes closed state, as evident across both frequency and time-frequency decompositions.

Our results suggests that signals traveling along the corpus callosum either produce or are in some way requisite for alpha rhythm generation. This finding is very exciting and supportive of the novel theory proposed under this award. This may be due to suppression or a desynchronization of activity/spike volleys. This provides important proof of concept that activity in white matter is synchronized, that TUS can be used for WM-frequency mapping, and for our ephaptic coupling model.

At the time of writing, numerous jobs have been submitted to the computer cluster to further analyze these data including group level alpha peak statistics for each EEG segment, and group level GLM analysis. The PI is committed to finishing this analysis and publishing this work.

DISTRIBUTION A: Distribution approved for public release.

OBJECTIVE 3: Record Neural Activity *in vivo* in Rodent White Matter Tracts (Originally Future Research)

I. Introduction

Although initially not included in the objectives of this proposal, we were able to successfully collect data on this future aim. The goal of this objective was to collect electrophysiologic measurements in rodent white matter to test for 1) the presence of synchronized 'spike volleys' in rodent white matter (ephaptic coupling), and 2) determine whether signals in white matter also follow a 1/f spectral density. Electrophysiology recordings in white matter are very rare for a number of reasons. First, most electrophysiologists are interested in studying voltage fluctuations in neurons in either gray matter or deep nuclei (e.g., amygdala). Second, most electrodes are specifically designed for low-resistivity milieu. Thus, most electrophysiologists hear 'silence' when electrodes are advanced through white matter tissue.

II. Methods

Male Long Evans rats (n=6) underwent neurosurgical placement of electrodes in white matter fiber bundles superior to hippocampus with 32-channel custom electrode with contacts spaced along 23.15 mm Neuro Probe-On-Board electrodes (IDAX Microelectronics) under deep isobutane anesthesia in accordance with NIH standard for care and use of laboratory animals and the Animal Research Council.

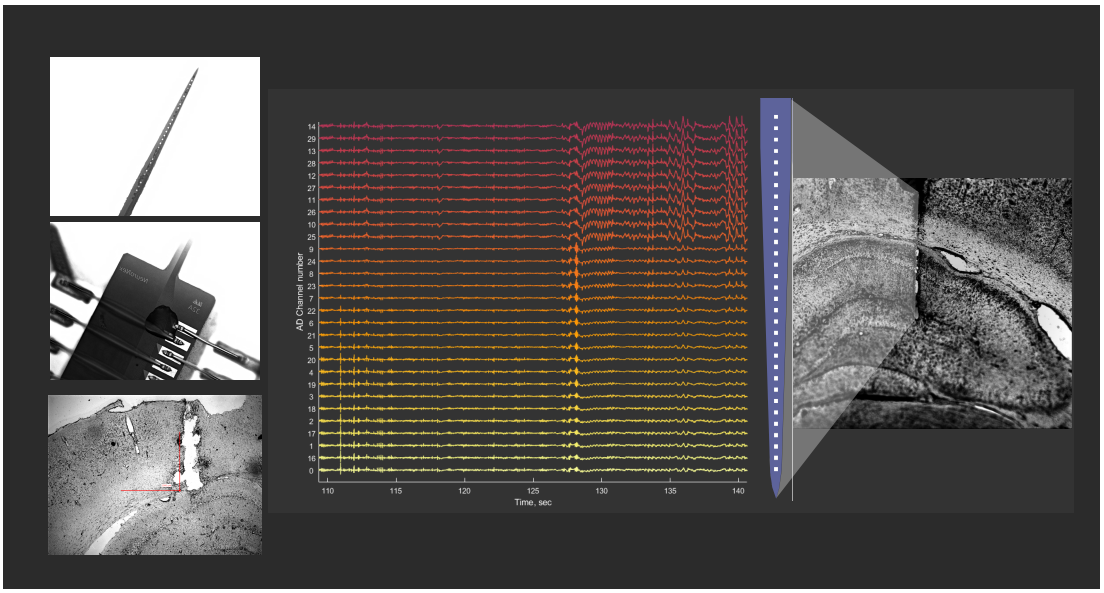


Figure 19: (Top left) Custom electroplating of electrode for recording in white matter. (Middle left) Our amplifier device for recording signals. (Lower left) histology image of neurosurgical placement in white matter confirmed through a high frequency pulse. (Right) Electrode coverage allowed recordings in both white matter and gray matter.

DISTRIBUTION A: Distribution approved for public release.

Importantly, this placement provided access to both white matter and gray matter recordings, given the spacing of the electrode contacts (**Figure 19**). All data were recorded at 20kHz in awake behaving animals, across 10 sec intervals for a minimum of 3 blocks per animal.

Following all behavioral experimentation, rodents were euthanized and a high frequency pulse was administered to heat tissue for subsequent histological staining, and verification of electrode location. Thereafter, Diffusion MRI imaging of rodent brains took place overnight on the 7 Tesla Bruker animal scanner at NYU Langone Health.

Statistical Analysis

All electrode data were first imported from the Intan device, and segmented into 5 second intervals. Spectral decompositions were performed on these windows to determine the extent to which log-linear 1/f signaling takes place in white matter tracts. Thereafter, Morlet wavelet decompositions were performed on each 10sec recording for each electrode. The time-frequency analysis was performed to determine if broad spectral entrainment of spikes traveling along white matter tracts is evident in these recordings.

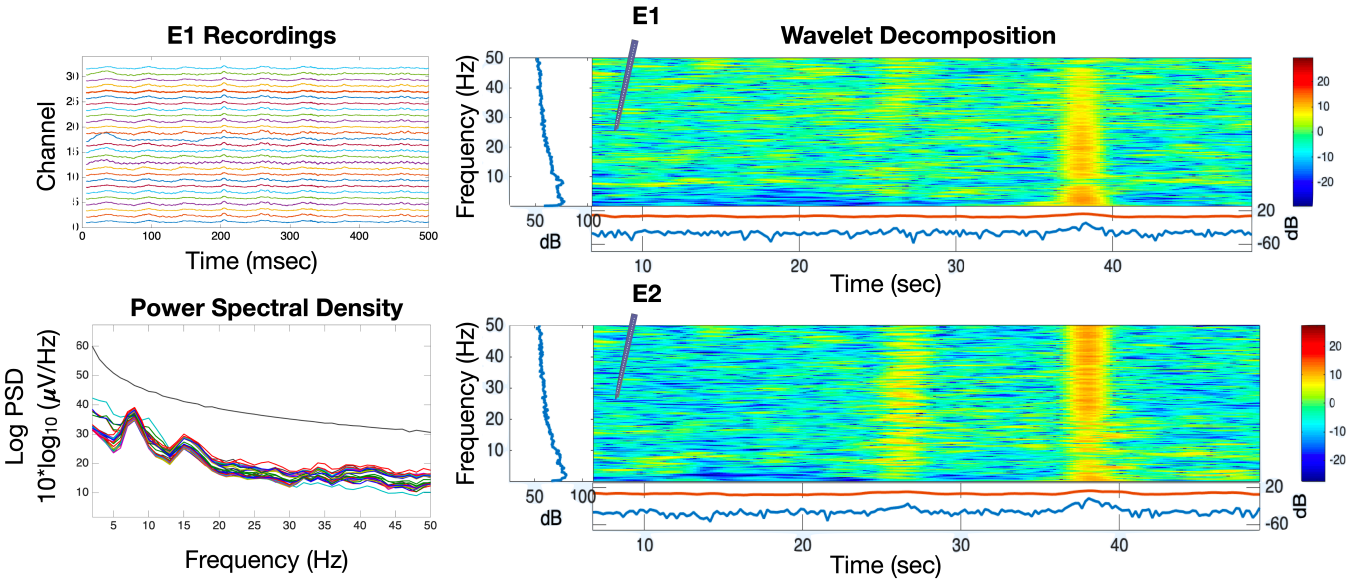


Figure 20: Upper Left) Time domain recordings from microelectrodes implanted in corpus callosum (CC) in awake behaving Long Evans rat sampled at 20,000 Hz., and Lower Left) corresponding Power spectral densities calculated across electrodes in white matter. Right) Upper and lower images are Morlet wavelet decompositions for selected white matter channels from microelectrodes E1 and E2 at distinct location in CC tract. Decompositions show broad band entrainment.

DISTRIBUTION A: Distribution approved for public release.

III. Results to date, Discussion & Ongoing Work

White matter electrode recordings in rodents are very rare. The PI of this grant could only find one paper in the literature that reported this type of work, and this study used electrodes which were not well suited for the high resistivity in white matter. Visual inspection of this data indeed shows a prominent 1/f spectral signature across channels in white matter tracts, with a slope that resembles that of observed dynamics in many scale free 1/f signatures of biological computation. Furthermore, the Wavelet decomposition shows that broad spectrum entrainment of volleys (or cross frequency coupling) across a variety of velocities (frequencies) is evident (**Figure 20**).

Future Proposed Analysis

We propose to analyze synchronized spike volleys in white matter as follows. First, we will define a spike volley as the coincidence of local field potential fluctuations being 3 standard deviations above the mean of all data across all channels, and occurring across more that 3 channels. A preliminary sequence score will be computed for each event as the correlation of time and position, as weighted by the posterior probability, as done in (Grossmark et al. 2016). Separately, 1000 null (shuffled) firing rate-by-position data sets were constructed by generating spikes drawn randomly from independent firing rate distributions. A second time-bin-shuffle will be performed by permuting the order of 20 ms time bins for each event. These null data sets will subsequently be used to generate sequence Z-scores, defined as the absolute value of the weighted-correlation relative to the expected absolute null weighted correlation distribution.

In a subsequent analysis, these null data distributions will be compared to the observed data distributions, by first smoothing these data with a moving average window, and computing the Kullback-Leibler (KL) divergence. KL divergence was computed in both directions (e.g., D_{KL} (P || Q), D_{KL} (Q || P)), to compute distance scores between null distributions and empirical recordings from gray and white matter.

Cable Model and Estimating Ephaptic Strength

These data and our computational model (Objective 1) readily lend themselves to future analyses of these data. The dMRI data collected in these rats can be analyzed and morphometric properties of each white matter tracts derived, as was done for the HCP data in objective 1 of this proposal. Rats have mostly lissencephalic brains, and though the percentage of unmyelinated neurons is mostly phylogenetically conserved, empirical data from Wang et al. (2008) shows that unmyelinated neurons make up a larger proportion of axons compared to humans.

Thus, these data are readily available, and our cable model can be readily applied to estimate the strength of ephaptic interactions and axonal cross-talk in vivo. Importantly, ephaptic interactions and the broad signal entrainment, observed here, may represent a new way of conceptualizing neural coding and information processing in the brain.

DISTRIBUTION A: Distribution approved for public release.

DELIVERABLES/ RESEARCH PRODUCTS

Manuscripts/Publications (in press)

The Air Force was thanked and acknowledged in all of the following publications:

Saeidi, M, Karwoowski, W., Farahani, FV, Fiok, K, Sawyer, BD,, Hancock, P, **Douglas, PK** "Decoding Task-Based fMRI Data with Graph Neural Networks, Considering Individual Differences," Brain Sciences 12(8):1094 (2022)

Larios-Dutta, C, Cristov-Moore, L, Ombao, H, **Douglas, PK** "Neuroprotection in Late Life ADHD: A Review of Pharmacotherapy and Phenotype across the Lifespan" Frontiers in Human Neuroscience. 16 : 938501 (2022)

Farahani, FV, Fiok, K, Lahijanian, B, Karwowski, W, **Douglas, PK.** "Explainable AI: A review of applications to neuroimaging data" *Frontiers in Neuroscience* 16: 2022, (2022) DOI: 10.3389/fnins.2022.906290

Chrstov-Moore, L, Iacaboni, M, Reggente, N, Schoeller, F, **Douglas, PK** , Kaplan, J, Damasio, AR, "Preventing Antisocial Robots: A Pathway to Artificial Empathy" *Science Robotics* (2023)

Farahani, FV, D'Esposito, M, Bettzel, RF, Fafowicz, M, Bohaterewicz, B, Marek, T, **Douglas, PK**, Karwowski, W, "Diurnal variations of resting-state fMRI data: A graph-based analysis" *NeuroImage 256: 119246* (2022)

The PI would like to thank the Air Force for funding, which helped generally support the PI while completing the following manuscripts and conference papers, though this award mechanism was not acknowledged. In some cases, this was because the format of the publication (e.g., book chapter) did not have an acknowledgment section, and in other cases, the work had been submitted prior to the award.

Douglas, PK, Farahani, FV, Anderson, A, Giles, J., "Sparse and Data-Driven Methods for Concurrent EEG-fMRI" Book Chapter in EEG-fMRI, Editors: Christoph Mulert, Louis Lemieux (2023)

Huang, Y, Barham, C, **Douglas, PK** "Triadic Temporal Exponential Random Graph Models" *NeurIPS - Temporal Graph Learning Workshop* (2022)

DISTRIBUTION A: Distribution approved for public release.

Vice, J, **Douglas, PK**, Sukthankar, G, "Leveraging Evolutionary Algorithms for Feasible Hexapod Locomotion Across Uneven Terrain", *35th International FLAIRS Conference* (2022)

Anderson, A, Diaz-Santos, S, Dang, B, Kaur, P, Lyden, P, Buxton, R, **Douglas, PK**, Bilder, RM, Esfandiari, M, Friston, KJ, Nookala, U, Bookheimer, SY "Hemodynamic latency is associated with reduced intelligence across the lifespan: an fMRI DCM study of aging, cerebrovascular integrity, and cognitive ability" *Brain Structure Function* 225:1705-1717 (2020)

Choupan, J, **Douglas, PK**, Gal, Y, Cohen, MS, Reutens, D, Yang, Z, "Temporal Embedding and Spatiotemporal Feature Selection Boost Multi-voxel Pattern Analysis Decoding Accuracy" *J Neurosci Methods*. 1(245):108826 (2020)

Douglas, PK & Farahani, F, "On the Similarity of Deep Learning Representations Across Didactic and Adversarial Examples" *NeurIPS- MED Workshop* (2020)

Manuscripts in preparation

The Air Force will be thanked and acknowledged in all of the following manuscripts as they are submitted for publication. The PI is committed to finalizing all analysis and submitting the following papers for publication:

PAPER 1: Douglas, PK, Lemieux, L. "White Matter Structure Predicts 1/f Spectra: A Cable Theoretic Generative Model" (in prep)

Brief Summary:

This manuscript, in preparation, will describe our findings from objective 1, specifically the building of a novel generative model for spike volleys in white matter fascicles to test and estimate the strength of ephaptic coupling in human brain white matter, under the hypothesis that signals traveling along white matter follow a 1/f log linear spectral distribution. Given that 1/f characteristics are a ubiquitous property of biological computation - across levels of abstraction, it seems biologically plausible that the dynamics of action potentials would also conform to this relationship. Furthermore, our preliminary data from Objective 3 shows 1/f signatures measured in vivo in rat white matter.

Overall, this generative model may provide important evidence for ephaptic coupling in the central nervous system. This model can also be used to make predictions about signal

DISTRIBUTION A: Distribution approved for public release.

latency across networks and rhythms in the brain. Latency estimates may prove crucial for identifying seizure onset zones in epilepsy, vastly improving EEG source localization, and opening up new solutions for BCI devices.

PAPER 2: Douglas, PK, Cristov-Moore, L, Blair, G., Alazarmi, P, Spivak, N, Reggente, N., Lemieux, L., Cain, J, "Transcranial Ultrasound Applied to Corpus Callosum extinguishes EEG Alpha Peak" (in prep)

Brief Summary:
The origin of the alpha rhythm in the brain has remained elusive and controversial for nearly a century. In this paper, we will provide strong supporting evidence that demonstrates that white matter signaling along the corpus callosum is a critical component, requisite for the generation of the alpha rhythm. This is in sharp contrast to the classic view that thalami-cortical interactions generate the alpha rhythm.

This is important because the alpha rhythm is known to play an important role in attention and the ability to focus on relevant information, allowing the brain to filter out distracting stimuli. It is also a crucial finding as it calls into question the classic orthodoxy in the field of EEG, specifically the Dipolar model used by generations of neuroscientists. This model suggests that we are only measuring superficial gray matter signals with this EEG. With this new information, we may be able to peer deeper into the brain using a noninvasive tool.

3.) **Douglas, PK,** Blair, G, Fenton, A, "Evidence for Axonal Cross-Talk in Rodent White Matter" (in prep)

Brief Summary:
We have begun the preparation of a third paper, which will detail our findings from objective 3. Specifically, it will describes the in vivo electrophysiology recordings in Long Evans rat white matter tracts. Following all electrophysiology recordings, rat brains were imaged overnight on a 7T MRI Animal scanner, and diffusion MRI images were collected. The results of this paper will show evidence for synchronized spike volleys - for the first time - in white matter tracts. Our ongoing statistical analysis will be quantifying spike volley synchrony, 1/f characteristic in white matter spectral decompositions, and leveraging our cable modeling approach in objective 1 to estimate the strength of ephaptic coupling in vivo from electrophysiology recordings in white matter fiber alongside the diffusion MRI data collected in these animals.

Conference Abstracts/Papers
Funding from this award helped directly support the following conference short paper:

DISTRIBUTION A: Distribution approved for public release.

Douglas, PK, Vice, J, Blair, G, "A White Matter Ephaptic Coupling Model for 1/f Spectral Densities", *Computational and Systems Neuroscience, Cosyne (Conference Paper, Peer-Reviewed)* (2022)

Conference Lecture

The PI of this award thanked the Air Force for funding in each of the following invited conference lectures and symposia:

2023	Organization for Human Brain Mapping Meeting (OHBM) - Symposium Lecture (Montreal) "Advances in EEG Generative Models and Multimodal EEG-fMRI"
2023	IEEE - ICASSP Meeting, DSLW: Unraveling the Brain (Rhodes) "Explainable AI for Neuroimaging"
2023	IEEE Brain Computer Interface IEEE Winter Conference (Korea) "Towards a white matter ephaptic coupling model for EEG Spectral Densities"
2023	Institute of Pure & Applied Mathematics (IPAM) - Explainable AI Workshop "Exploring XAI Techniques for Neuroimaging"
2022	Keynote, CoSyne MAIN Meeting (Portugal) "Exploring a White Matter Ephaptic Coupling Model for 1/f"
2021	BioRTC TrEND Meeting (virtual) "Interpretable Deep Learning for Exploratory Research"
2020	Montreal Artificial Intelligence & Neuroscience (MAIN) Meeting (virtual) "Introduction to Interpreting Deep Learning"
2020	Organization for Human Brain Mapping Meeting (OHBM), Pattern Recognition in Neuroimaging (PRNI) Educational Workshop, "Deep Learning for Neuroimaging: An Introduction"
2020	National Institute of Health (NIH -NIMH) "Explainable AI for Neuroimaging: Challenges and Future Directions"
2020	University of Zurich Neuroeconomics Speaker Series "Transparency In Deep Learning for Neuroimaging"

DISTRIBUTION A: Distribution approved for public release.

PARTICIPANTS & COLLABORATING ORGANIZATIONS

This project required an integration of expertise across multiple domains of study to include: acoustic and mechanical wave propagation, cable and communication theory, volume conductance models, finite element modeling, electromagnetism, multimodal neuroimaging, material science, and functional neuroanatomy.

The PI of this project would like to thank the following collaborators that contributed time and specialized knowledge towards the project objectives.

Andre Fenton & Garrett Blair (NYU, Neuroimaging and recordings in rodents)

The Fenton lab at NYU provided in kind support for all animal experimentation in Objective 3. This include animal husbandry,

Taylor Kuhn, Normal Spivak (IACS, UCLA, TUS & Arteriole Spin Labeling)

Taylor Kuhn kindly shared MRI ASL sequences for this study, and provided critical guidance on the parameters used for TUS sonication. Normal Spivak provided materials testing of all sham stand-off pad material candidates, and testing of materials for construction of a new EEG sensor to be build by Magstim EGI.

Josh Cain, Pardis Azrami-Pour (IACS, Cedars Sinai, Data Collection TUS-EEG)

Pardis was a student who volunteered to assist with all subject recruitment and data collection, which required numerous hours for each subject. Thus, this grant helped support the training of advancing the skills of a junior scientist. Josh Cain ran TUS-EEG experiments on subjects who received sonication to the thalamus.

EGI Magstim

MagStim provided, in kind, one new 256 electrode EEG sensor net, build with materials that allowed ultrasound to pass through. Importantly, this provided the opportunity to collect “online” EEG data during sonication. Many thanks to Bill McSwain who built this high density EEG sensor net for TUS and this project specifically.

Mark & Sam Schaffer (Brainsonix, Drexel University)

Mark and Sam Schaffer provided materials testing and development of the sham stand-off pads for our control condition.

Robert Barry (University of Wollongong, Australia)

Prof. Barry kindly provided his novelty sound library for our EEG odd-ball paradigm.

DISTRIBUTION A: Distribution approved for public release.

Yifan Huang (UCF IST)
Yifan assisted with extracting morphometric properties from the dMRI data across the HCP data set. Yifan was a student, and thus this provided the opportunity for training.

Klaus Robert-Muller (IPAM, TU Berlin)
Klaus Robert-Muller has provided exceptional guidance on how to build a novel EEG forward model that incorporates the anisotropic properties of white matter - a new potential source for EEG generation. This will be the subject of future work. He has also provided guidance on the circle packing problem using soft margin boundaries.

DISTRIBUTION A: Distribution approved for public release.

ADDITIONAL ACKNOWLEDGEMENTS

This project required an integration of expertise across multiple domains of study to include: acoustic and mechanical wave propagation, cable and communication theory, volume conductance models, finite element modeling, electromagnetism, multimodal neuroimaging, material science, and functional neuroanatomy. The PI of this project would like to thank the following collaborators that contributed time and specialized knowledge towards the project objectives.

Hal Greenwald (AFOSR)
overall project guidance and wonderful support

Stefan Haufe (Bernstein Center for Computational Neuroscience)
EEG/MEG Source Modeling

Eric Miller (Tufts)
Ultrasound & Acoustic Wave Modeling

David Douglas (Harvard)
neuroradiology

Rene Hartig (Max Planck Tubingen)
neuroanatomy of white matter tracts

Kai Miller (Mayo Clinic)
dipole sources and higher order geometries

Sasha Bystritsky (Brainsonix)
guidance on acoustic Parameters for TUS

Susan Bookheimer (UCLA)
behavioral paradigms

Mark Crawley (Brainbox)
NeuroFUS system

Robert Douglas (USASB)
project guidance

Avi Adhikari (UCLA)
rodent white matter electrophysiology

Christophe Phillip (U Liege)
Anisotropic EEG lead field models

Grace Bochenek (UCF IST)
project guidance

DISTRIBUTION A: Distribution approved for public release.

TUS is quite possibly the most exciting new tool for human brain research. The research supported by this AFOSR CCN grant provided the opportunity for the PI to be a part of this groundbreaking work. The results across computational modeling, and multiple scales of empirical data provide very exciting evidence in support of the theory that white matter signaling may contribute to EEG/MEG biorhythms.

This work would not have been possible without support from AFOSR. The PI is incredibly grateful for this incredible support, which has jump-started and accelerated this ground-breaking work.

DISTRIBUTION A: Distribution approved for public release.

Bibliography

Adrian, E. D. and B. H. C. Matthews (1934). "The interpretation of potential waves in the cortex." The Journal of Physiology **81**(4): 440-471.

Adrian, E. D. and K. Yamagiwa (1935). "THE ORIGIN OF THE BERGER RHYTHM." Brain **58**(3): 323-351.

Anastassiou, C. A. and C. Koch (2015). "Ephaptic coupling to endogenous electric field activity: why bother?" Current Opinion in Neurobiology **31**: 95-103.

Anastassiou, C. A., R. Perin, H. Markram and C. Koch (2011). "Ephaptic coupling of cortical neurons." Nature Neuroscience **14**(2): 217-223.

Andersen, P., T. V. Bliss and K. K. Skrede (1971). "Unit analysis of hippocampal population spikes." Exp. Brain. Res. **13**: 208-221.

Andrietti, F. and G. Bernardini (1984). "Segmented and "equivalent" representation of the cable equation." Biophysical Journal **46**(5): 615-623.

Arvanitaki, A. (1942). "Effects evoked in an axon by the activity of a contiguous one." Journal of Neurophysiology **5**(2): 89-108.

Basser, P. J. (1993). "Cable equation for a myelinated axon derived from its microstructure." Medical & Biological Engineering & Computing **31**(S1): S87-S92.

Bastos, Andre M., W. M. Usrey, Rick A. Adams, George R. Mangun, P. Fries and Karl J. Friston (2012). "Canonical Microcircuits for Predictive Coding." Neuron **76**(4): 695-711.

Berger, H. (1929). "Über das Elektrenkephalogramm des Menschen." Archiv für Psychiatrie und Nervenkrankheiten **87**(1): 527-570.

Beurle, R. L. (1956). "Properties of a mass of cells capable of regenerating pulses." Philosophical Transactions of the Royal Society of London. Series B, Biological Sciences **240**(669): 55-94.

Bosman, Conrado A., J.-M. Schoffelen, N. Brunet, R. Oostenveld, Andre M. Bastos, T. Womelsdorf, B. Rubehn, T. Stieglitz, P. De Weerd and P. Fries (2012). "Attentional Stimulus Selection through Selective Synchronization between Monkey Visual Areas." Neuron **75**(5): 875-888.

Braitenberg, V. (1978). Cell Assemblies in the Cerebral Cortex. Theoretical Approaches to Complex Systems. R. Heim and G. Palm. Berlin, Heidelberg, Springer Berlin Heidelberg. **21:** 171-188.

Braitenberg, V. and A. Schuz (2002). The Human Cortical White Matter: Quantitative Aspects of Cortico-Cortical Long-Range Connectivity. Cortical Areas. R. Miller and A. Schüz, CRC Press. **20020530:** 377-385.

Bushberg, J. T., J. A. Seibert, E. M. Leidholt and J. M. Boone (2021). The essential physics of medical imaging.

Buzsáki, G., C. A. Anastassiou and C. Koch (2012). "The origin of extracellular fields and currents — EEG, ECoG, LFP and spikes." Nature Reviews Neuroscience **13**(6): 407-420.

Bystritsky, A., A. S. Korb, P. K. Douglas, M. S. Cohen, W. P. Melega, A. P. Mulgaonkar, A. DeSalles, B.-K. Min and S.-S. Yoo (2011). "A review of low-intensity focused ultrasound pulsation." Brain Stimulation **4**(3): 125-136.

DISTRIBUTION A: Distribution approved for public release.

Caminiti, R., F. Carducci, C. Piervincenzi, A. Battaglia-Mayer, G. Confalone, F. Visco-Comandini, P. Pantano and G. M. Innocenti (2013). "Diameter, Length, Speed, and Conduction Delay of Callosal Axons in Macaque Monkeys and Humans: Comparing Data from Histology and Magnetic Resonance Imaging Diffusion Tractography." Journal of Neuroscience **33**(36): 14501-14511.

Caton, R. (1875). "The electric currents of the brain." **2**: 278.

Cooper, R., A. L. Winter, H. J. Crow and W. G. Walter (1965). "Comparison of subcortical, cortical and scalp activity using chronically indwelling electrodes in man." Electroencephalography and Clinical Neurophysiology **18**(3): 217-228.

Cooray, G., B. Sengupta, P. K. Douglas and K. J. Friston (2016). "Dynamic causal modelling of electrographic seizure activity using Bayesian belief updating." Neuroimage **125**: 1142-1154.

Cooray, G. K., B. Sengupta, P. Douglas, M. Englund, R. Wickstrom and K. Friston (2015). "Characterising seizures in anti-NMDA-receptor encephalitis with dynamic causal modelling." NeuroImage **118**: 508-519.

Creutzfeldt, O. D. (1977). "Generality of the functional structure of the neocortex." Naturwissenschaften **64**(10): 507-517.

David, O. and K. J. Friston (2003). "A neural mass model for MEG/EEG." NeuroImage **20**(3): 1743-1755.

Deco, G., V. K. Jirsa, P. A. Robinson, M. Breakspear and K. Friston (2008). "The Dynamic Brain: From Spiking Neurons to Neural Masses and Cortical Fields." PLoS Computational Biology **4**(8): e1000092.

Dell'Italia, J., J. L. Sanguinetti, M. M. Monti, A. Bystritsky and N. Reggente (2022). "Current State of Potential Mechanisms Supporting Low Intensity Focused Ultrasound for Neuromodulation." Frontiers in Human Neuroscience **16**: 872639.

Denève, S. and C. K. Machens (2016). "Efficient codes and balanced networks." Nature Neuroscience **19**(3): 375-382.

Douglas, P. K. and D. B. Douglas (2019). Reconsidering Spatial Priors In EEG Source Estimation : Does White Matter Contribute to EEG Rhythms? 2019 7th International Winter Conference on Brain-Computer Interface (BCI), IEEE.

Douglas, R. J. and K. A. Martin (1991). "A functional microcircuit for cat visual cortex." The Journal of Physiology **440**(1): 735-769.

Ebersole, J. S. (1997). "Defining Epileptogenic Foci: Past, Present, Future." Journal of Clinical Neurophysiology **14**(6): 470-483.

Eccles, J. C. (1951). "Interpretation of action potentials evoked in the cerebral cortex." Electroencephalography and Clinical Neurophysiology **3**(4): 449-464.

Einevoll, G. T., K. H. Pettersen, A. Devor, I. Ulbert, E. Halgren and A. M. Dale (2007). "Laminar Population Analysis: Estimating Firing Rates and Evoked Synaptic Activity From Multielectrode Recordings in Rat Barrel Cortex." Journal of Neurophysiology **97**(3): 2174-2190.

Fry, F. J. (1958). "Precision high intensity focusing ultrasonic machines for surgery." American Journal of Physical Medicine **37**(3): 152-156.

DISTRIBUTION A: Distribution approved for public release.

Glasser, M. F., S. N. Sotiropoulos, J. A. Wilson, T. S. Coalson, B. Fischl, J. L. Andersson, J. Xu, S. Jbabdi, M. Webster, J. R. Polimeni, D. C. Van Essen and M. Jenkinson (2013). "The minimal preprocessing pipelines for the Human Connectome Project." NeuroImage **80**: 105-124.

Goldwyn, J. H. and J. Rinzel (2016). "Neuronal coupling by endogenous electric fields: cable theory and applications to coincidence detector neurons in the auditory brain stem." Journal of Neurophysiology **115**(4): 2033-2051.

Güllmar, D., J. Haueisen and J. R. Reichenbach (2010). "Influence of anisotropic electrical conductivity in white matter tissue on the EEG/MEG forward and inverse solution. A high-resolution whole head simulation study." NeuroImage **51**(1): 145-163.

Hodgkin, A. L. and W. A. H. Rushton (1946). "The electrical constants of a crustacean nerve fibre." Proceedings of the Royal Society of London. Series B - Biological Sciences **133**(873): 444-479.

Hursh, J. B. (1939). "CONDUCTION VELOCITY AND DIAMETER OF NERVE FIBERS." American Journal of Physiology-Legacy Content **127**(1): 131-139.

Izhikevich, E. M. and G. M. Edelman (2008). "Large-scale model of mammalian thalamocortical systems." Proceedings of the National Academy of Sciences **105**(9): 3593-3598.

Jack, J. J. B., D. Noble and R. W. Tsien (1988). Electric current flow in excitable cells. Oxford, Clarendon Press.

Jansen, B. H. and V. G. Rit (1995). "Electroencephalogram and visual evoked potential generation in a mathematical model of coupled cortical columns." Biological Cybernetics **73**(4): 357-366.

Katz, B. and O. H. Schmitt (1940). "Electric interaction between two adjacent nerve fibres." The Journal of Physiology **97**(4): 471-488.

Klimesch, W., P. Sauseng and S. Hanslmayr (2007). "EEG alpha oscillations: The inhibition–timing hypothesis." Brain Research Reviews **53**(1): 63-88.

Krogsrud, S. K., A. M. Fjell, C. K. Tamnes, H. Grydeland, L. Mork, P. Due-Tonnessen, A. Bjornerud, C. Sampaio-Baptista, J. Andersson, H. Johansen-Berg and K. B. Walhovd (2016). "Changes in white matter microstructure in the developing brain--A longitudinal diffusion tensor imaging study of children from 4 to 11years of age." Neuroimage **124**(Pt A): 473-486.

Lee, H.-H., K. Yaros, J. Veraart, J. L. Pathan, F.-X. Liang, S. G. Kim, D. S. Novikov and E. Fieremans (2019). "Along-axon diameter variation and axonal orientation dispersion revealed with 3D electron microscopy: implications for quantifying brain white matter microstructure with histology and diffusion MRI." Brain Structure and Function **224**(4): 1469-1488.

Lee, W., H.-C. Kim, Y. Jung, Y. A. Chung, I.-U. Song, J.-H. Lee and S.-S. Yoo (2016). "Transcranial focused ultrasound stimulation of human primary visual cortex." Scientific Reports **6**(1): 34026.

Liewald, D., R. Miller, N. Logothetis, H.-J. Wagner and A. Schüz (2014). "Distribution of axon diameters in cortical white matter: an electron-microscopic study on three human brains and a macaque." Biological Cybernetics **108**(5): 541-557.

Logothetis, N. K., C. Kayser and A. Oeltermann (2007). "In Vivo Measurement of Cortical Impedance Spectrum in Monkeys: Implications for Signal Propagation." Neuron **55**(5): 809-823.

Lopes da Silva, F. (2013). "EEG and MEG: Relevance to Neuroscience." Neuron **80**(5): 1112-1128.

DISTRIBUTION A: Distribution approved for public release.

Lopes da Silva, F. H. (2023). EEG: Origin and Measurement. EEG-fMRI: Physioological Basis, Technique, aan Applications. Switzerland, Springer Nature**:** 23-48.

Lopes Da Silva, F. H. and W. Storm Van Leeuwen (1977). "The cortical source of the alpha rhythm." Neuroscience Letters **6**(2-3): 237-241.

Lorente De Nó, R. (1947). "Action potential of the motoneurons of the hypoglossus nucleus: ACTION POTENTIAL OF MOTONEURONS." Journal of Cellular and Comparative Physiology **29**(3): 207-287.

McColgan, P., S. Helbling, L. Vaculčiaková, K. Pine, K. Wagstyl, F. M. Attar, L. Edwards, M. Papoutsi, Y. Wei, M. P. Van Den Heuvel, S. J. Tabrizi, G. Rees and N. Weiskopf (2021). "Relating quantitative 7T MRI across cortical depths to cytoarchitectonics, gene expression and connectomics." Human Brain Mapping **42**(15): 4996-5009.

McNeal, D. R. (1976). "Analysis of models for external simulation of axons." IEEE Transactions on Biomedical Engineering **23**(4): 329-337.

Moran, R., D. A. Pinotsis and K. Friston (2013). "Neural masses and fields in dynamic causal modeling." Frontiers in Computational Neuroscience **7**.

Mostapha, M. and M. Styner (2019). "Role of deep learning in infant brain MRI analysis." Magnetic Resonance Imaging **64**: 171-189.

Movahedian Attar, F., E. Kirilina, D. Haenelt, K. J. Pine, R. Trampel, L. J. Edwards and N. Weiskopf (2020). "Mapping Short Association Fibers in the Early Cortical Visual Processing Stream Using In Vivo Diffusion Tractography." Cerebral Cortex **30**(8): 4496-4514.

Neishabouri, A. and A. A. Faisal (2014). "Saltatory conduction in unmyelinated axons: clustering of Na(+) channels on lipid rafts enables micro-saltatory conduction in C-fibers." Frontiers in Neuroanatomy **8**: 109.

Nie, J., L. Guo, K. Li, Y. Wang, G. Chen, L. Li, H. Chen, F. Deng, X. Jiang, T. Zhang, L. Huang, C. Faraco, D. Zhang, C. Guo, P.-T. Yap, X. Hu, G. Li, J. Lv, Y. Yuan, D. Zhu, J. Han, D. Sabatinelli, Q. Zhao, L. S. Miller, B. Xu, P. Shen, S. Platt, D. Shen, X. Hu and T. Liu (2012). "Axonal Fiber Terminations Concentrate on Gyri." Cerebral Cortex **22**(12): 2831-2839.

Nunez, P. L., L. Reid and R. G. Bickford (1978). "The relationship of head size to alpha frequency with implications to a brain wave model." Electroencephalography and Clinical Neurophysiology **44**(3): 344-352.

Nunez, P. L. and R. Srinivasan (2006). "A theoretical basis for standing and traveling brain waves measured with human EEG with implications for an integrated consciousness." Clinical Neurophysiology **117**(11): 2424-2435.

Oh, S.-J., J. M. Lee, H.-B. Kim, J. Lee, S. Han, J. Y. Bae, G.-S. Hong, W. Koh, J. Kwon, E.-S. Hwang, D. H. Woo, I. Youn, I.-J. Cho, Y. C. Bae, S. Lee, J. W. Shim, J.-H. Park and C. J. Lee (2019). "Ultrasonic Neuromodulation via Astrocytic TRPA1." Current Biology **29**(20): 3386-3401.e3388.

Oishi, M., H. Otsubo, S. Kameyama, N. Morota, H. Masuda, M. Kitayama and R. Tanaka (2002). "Epileptic Spikes: Magnetoencephalography versus Simultaneous Electrocorticography." Epilepsia **43**(11): 1390-1395.

Pinotsis, D. A., R. J. Moran and K. J. Friston (2012). "Dynamic causal modeling with neural fields." NeuroImage **59**(2): 1261-1274.

DISTRIBUTION A: Distribution approved for public release.

Rall, W. (2006). "Theory of Physiological Properties of Dendrites." Annals of the New York Academy of Sciences **96**(4): 1071-1092.

Riera, J. J., T. Ogawa, T. Goto, A. Sumiyoshi, H. Nonaka, A. Evans, H. Miyakawa and R. Kawashima (2012). "Pitfalls in the dipolar model for the neocortical EEG sources." Journal of Neurophysiology **108**(4): 956-975.

Roebroeck, A., A. K. Seth and P. A. Valdés-Sosa (2011). "Causal Time Series Analysis of Functional Magnetic Resonance Imaging Data." JMLR W&CP **12**: 65-94.

Rosenblueth, A. (1941). "THE STIMULATION OF MYELINATED AXONS BY NERVE IMPULSES IN ADJACENT MYELINATED AXONS." American Journal of Physiology-Legacy Content **132**(1): 119-128.

Schaworonkow, N. and B. Voytek (2021). "Longitudinal changes in aperiodic and periodic activity in electrophysiological recordings in the first seven months of life." Developmental Cognitive Neuroscience **47**: 100895.

Scherg, M. (1990). "Fundamentals of Dipole Source Potential Analysis." In: Advances in Audiology, 6, Basel, Karger: 40-69.

Schmidt, H., G. Hahn, G. Deco and T. R. Knösche (2021). "Ephaptic coupling in white matter fibre bundles modulates axonal transmission delays." PLOS Computational Biology **17**(2): e1007858.

Schmidt, H. and T. R. Knösche (2022). "Modelling the effect of ephaptic coupling on spike propagation in peripheral nerve fibres." Biological Cybernetics **116**(4): 461-473.

Schwartz, W., B. Neumcke and R. Stampfli (1979). "Longitudinal Resistance of axoplasm in myelinated nerve fibers of the frog." Pflugers Arch Eur. J. Physiol. **379**(R41).

Sengupta, B. and M. B. Stemmler (2014). "Power Consumption During Neuronal Computation." Proceedings of the IEEE **102**(5): 738-750.

Sheheitli, H. and V. K. Jirsa (2020). "A mathematical model of ephaptic interactions in neuronal fiber pathways: Could there be more than transmission along the tracts?" Network Neuroscience (Cambridge, Mass.) **4**(3): 595-610.

Sotiropoulos, S. N., S. Moeller, S. Jbabdi, J. Xu, J. L. Andersson, E. J. Auerbach, E. Yacoub, D. Feinberg, K. Setsompop, L. L. Wald, T. E. J. Behrens, K. Ugurbil and C. Lenglet (2013). "Effects of image reconstruction on fiber orientation mapping from multichannel diffusion MRI: Reducing the noise floor using SENSE: Effects of dMRI Image Reconstruction on Fiber Orientations." Magnetic Resonance in Medicine **70**(6): 1682-1689.

Spruston, N. (2008). "Pyramidal neurons: dendritic structure and synaptic integration." Nature Reviews Neuroscience **9**(3): 206-221.

Stone, J. L. and J. R. Hughes (2013). "Early History of Electroencephalography and Establishment of the American Clinical Neurophysiology Society." Journal of Clinical Neurophysiology **30**(1): 28-44.

Tao, J. X., A. Ray, S. Hawes-Ebersole and J. S. Ebersole (2005). "Intracranial EEG Substrates of Scalp EEG Interictal Spikes." Epilepsia **46**(5): 669-676.

Tasaki, I. and W. H. Freygang (1955). "THE PARALLELISM BETWEEN THE ACTION POTENTIAL, ACTION CURRENT, AND MEMBRANE RESISTANCE AT A NODE OF RANVIER." The Journal of General Physiology **39**(2): 211-223.

DISTRIBUTION A: Distribution approved for public release.

Thatcher, R. W., P. J. Krause and M. Hrybyk (1986). "Cortico-cortical associations and EEG coherence: A two-compartmental model." Electroencephalography and Clinical Neurophysiology **64**(2): 123-143.

Trujillo, C. A., R. Gao, P. D. Negraes, J. Gu, J. Buchanan, S. Preissl, A. Wang, W. Wu, G. G. Haddad, I. A. Chaim, A. Domissy, M. Vandenberghe, A. Devor, G. W. Yeo, B. Voytek and A. R. Muotri (2019). "Complex Oscillatory Waves Emerging from Cortical Organoids Model Early Human Brain Network Development." Cell Stem Cell **25**(4): 558-569.e557.

Valdés-Hernández, P. A., A. Ojeda-González, E. Martínez-Montes, A. Lage-Castellanos, T. Virués-Alba, L. Valdés-Urrutia and P. A. Valdes-Sosa (2010). "White matter architecture rather than cortical surface area correlates with the EEG alpha rhythm." NeuroImage **49**(3): 2328-2339.

Voytek, B., M. A. Kramer, J. Case, K. Q. Lepage, Z. R. Tempesta, R. T. Knight and A. Gazzaley (2015). "Age-Related Changes in 1/ f Neural Electrophysiological Noise." The Journal of Neuroscience **35**(38): 13257-13265.

Wang, H., J. Wang, G. Cai, Y. Liu, Y. Qu and T. Wu (2021). "A Physical Perspective to the Inductive Function of Myelin—A Missing Piece of Neuroscience." Frontiers in Neural Circuits **14**: 562005.

Wang, S. S. H., J. R. Shultz, M. J. Burish, K. H. Harrison, P. R. Hof, L. C. Towns, M. W. Wagers and K. D. Wyatt (2008). "Functional Trade-Offs in White Matter Axonal Scaling." Journal of Neuroscience **28**(15): 4047-4056.

Waxman, S. G. and H. A. Swadlow (1977). "The conduction properties of axons in central white matter." Progress in Neurobiology **8**: 297-324.

Wilson, H. R. and J. D. Cowan (1972). "Excitatory and Inhibitory Interactions in Localized Populations of Model Neurons." Biophysical Journal **12**(1): 1-24.

Wolters, C. H., A. Anwander, X. Tricoche, D. Weinstein, M. A. Koch and R. S. MacLeod (2006). "Influence of tissue conductivity anisotropy on EEG/MEG field and return current computation in a realistic head model: A simulation and visualization study using high-resolution finite element modeling." NeuroImage **30**(3): 813-826.

Yoo, S., D. R. Mittelstein, R. C. Hurt, J. Lacroix and M. G. Shapiro (2022). "Focused ultrasound excites cortical neurons via mechanosensitive calcium accumulation and ion channel amplification." Nature Communications **13**(1): 493.

DISTRIBUTION A: Distribution approved for public release.